PURIFICATION AND DISPERSION OF NANOPARTICLES WITH 0-D, 1-D, AND 2-D GEOMETRIES

A Dissertation

by

XI ZHANG

Submitted to the Office of Graduate Studies of
Texas A&M University
in partial fulfillment of the requirements for the degree of

DOCTOR OF PHILOSOPHY

May 2012

Major Subject: Materials Science and Engineering

Purification and Dispersion of Nanoparticles with 0-D, 1-D, and 2-D Geometries

PURIFICATION AND DISPERSION OF NANOPARTICLES WITH 0-D, 1-D, AND 2-D GEOMETRIES

A Dissertation

by

XI ZHANG

Submitted to the Office of Graduate Studies of
Texas A&M University
in partial fulfillment of the requirements for the degree of

DOCTOR OF PHILOSOPHY

Approved by:

Chair of Committee,	Hung-Jue Sue
Committee Members,	John Gladysz
	Daniel Shantz
	Hongcai Zhou
Intercollegiate Faculty Chair,	Ibrahim Karaman

May 2012

Major Subject: Materials Science and Engineering

ABSTRACT

Purification and Dispersion of Nanoparticles with 0-D, 1-D, and 2-D Geometries.

(May 2012)

Xi Zhang, B.S., Wuhan University

Chair of Advisory Committee: Dr. Hung-Jue Sue

Nanoparticles (NPs) of different geometries, including 0-dimensional (0-D) ZnO QDs, 1-D carbon nanotubes (CNTs) and 2-D α-zirconium phosphate nanoplatelets (ZrP), have been purified and dispersed in various media. The individually dispersed ZnO QDs and ZrP can be easily purified by removing ions or dispersants. In the case of CNTs, more elaborate efforts are needed.

CNT is an important category of 1-D NPs with many desirable properties. These properties, however, are affected strongly by the dispersion state of CNTs, especially for single-walled CNTs (SWCNTs). Covalent and non-covalent techniques have been developed to disperse SWCNTs by interrupting secondary interactions between nanotubes. However, the application of SWCNTs processed by current dispersion technique is restricted by either the low yield or the property degradation.

To obtain purified and individually dispersed SWCNTS with preserved electronic state in large scale, SWCNTs have been first exfoliated with electrostatically tethered ZrP nanoplatelet dispersant. To remove the nanoplatelet dispersant, two approaches have then been developed: the ionic approach and the acid-mediated

approach. The ionic approach works by disrupting the electrostatic interaction between SWCNTs and ZrP with extra electrolytes and using non-ionic surfactants to stabilize SWCNTs. Two different mechanisms have been identified for monovalent and divalent cations, respectively. The acid-mediated approach is more versatile for choices of SWCNT stabilizer. When the above isolation procedures are optimized, over 90% of purified SWCNTs can be retrieved and stabilized in aqueous solution. The properties of the obtained SWCNTs are investigated extensively, showing that the electronic state and the structural integrity of SWCNTs are maintained. The acquired SWCNTs can be transferred into various kinds of solvents and polymer matrices. Possible applications include optoelectronic devices, reinforcement agent, and conductive fillers.

Individually dispersed SWCNTs can be further purified from the surfactants and stabilized in a good solvent without using surfactants, through the minimization of van der Waals (vdW) attraction. The same concept appears to hold true for stabilization of both purified 0-D QDs and 2-D nanoplatelets. With additional manipulation of ionic strength in solvent, the surfactant-free ZnO QDs can be progressively tuned to exhibit phase transitions similar to that of micro-spheres and even form colloidal crystals.

ACKNOWLEDGEMENTS

I would like to thank my committee chair, Prof. Hung-Jue Sue, and my committee members, Prof. John Gladysz, Prof. Daniel Shantz, and Prof. Benner for their guidance and support throughout the course of this research.

I thank Drs. Xin Wei, W. Neil Everett, Dazhi Sun, Chien-Chia Chu, Zhiping Luo, Han-soo Kim, Amanda Young and Daqiang Yuan for valuable discussion and technical assistance. Special thanks also go to Ms. Ann Ellis, Ms. Min Shuai, Ms. Haiqing Yao, Mr. Rick Littleton and Mr. Kevin. L. White for their help during my PhD research. I also want to extend my gratitude to all my friends and colleagues and the department faculty and staff for making my time at Texas A&M University a great experience.

Finally, thanks to my parents and my little sister for their tremendous patience and love.

NOMENCLATURE

Φ	Interatomic, intermolecular or interparticle potential
Φ_{vdw}	Interatomic, intermolecular or interparticle van der Waals potential
Φ_{min}	Interparticle potential at minimum separation
C	Coefficient for interatomic potential
d	Interatomic or interparticle distance
r	Radius of a particle
$2r$	Diameter of a particle
l	Length of a rod-like particle
t	Thickness of a plate-like particle
a	Lattice constant for cubic crystals
q	Scattering vector
θ	Scattering angle
φ	Volume fraction
ψ	Surface potential
ε	Relative dielectric constant (or permittivity)
σ	Surface charge density
λ	Wavelength
κ^{-1}	Debye length
A	Hamaker constant

T	Temperature
kT	Thermal energy
pKa	Acid dissociation constant
CMC	Critical micelle concentration
CNT	Carbon nanotube
SWCNT	Single-walled carbon nanotube
MWCNT	multi-walled carbon nanotube
QD	Quantum dot
NP	Nanoparticle

TABLE OF CONTENTS

CHAPTER Page

CHAPTER Page

Page

LIST OF FIGURES

FIGURE Page

FIGURE Page

FIGURE Page

FIGURE Page

LIST OF TABLES

CHAPTER I

INTRODUCTION

1.1 The Origin and Estimation of vdW Attraction

The balance between interparticle repulsion and vdW attraction determines the stability of colloidal particles.[1] According to Derjaguin-Landau-Verwey-Overbeek (DLVO) theory, the vdW force is always present and dominates at close proximity and eventually causes the aggregation of particles. The vdW attraction originates from the dipole-dipole interactions between atoms and molecules, including 1) permanent dipole-permanent dipole interaction (Keesom energy), 2) permanent dipole – induced dipole interaction (Debye energy); and 3) induced dipole – induced dipole interaction (London energy).[2] An interatomic or intermolecule van der Waals pair potential has a form of

$$\Phi_{vdW} = -C/d^6 \tag{1.1}$$

where d is the interatomic distance and C is the potential coefficent.[2-3]

Hamaker's summation principle indicates that the vdW force between two microscopic bodies can be estimated by integrating all pairwise combinations of intermolecular attraction. The resulting vdW interaction is usually given in terms of the conventional Hamaker constant

$$A = \pi^2 C \rho_1 \rho_2 \tag{1.2}$$

where ρ_1 and ρ_2 are the number of atoms per unit in the two bodies and C is the coefficient for interatomic potential.[3] The resulted macroscopic vdW force has a gener-

---

This dissertation follows the style of *Angewandte Chemie*.

al form of

$$\Phi_{vdW} = -A \text{ constant} \quad (1.3)$$

where the constant differs between different geometries.[2-3]

Interparticle vdW attraction can be compensated by electrical double layer repulsion or steric repulsion,[4] rendering the particles dispersed. This is often realized by capping the particles with ligands or surfactants. The surface decoration is especially important for manipulating NPs due to their fast kinetics.

1.2 History and Properties of NPs

The word "nanoparticle" has been used to describe particles with at least one sub-micron dimension in many cases. Compared with bulk materials, these particles have faster diffusion rate, larger surface-area-to-volume ratio and dimensions comparable to the wavelength of visible light, making them useful for fabrication of photonic crystals.[5] However, sub-10 nm NPs are more of interest to researchers for their interesting size-dependence of many physical and chemical properties like electro-optical,[6] electro-magnetic,[7] and thermodynamic properties.[8] By this definition, Faraday's colloidal gold (addressed to the Royal Society in 1857) is well acknowledged as the first record of the synthesis of NPs and the birth of modern nanotechnology.[9] Yet, the morphology of this colloidal gold had not been characterized until about 100 years afterwards, with the invention of transmission electron microscopy (TEM). Turkevich, in his report to the Discussion of the Faraday Society in 1951, identified that Faraday's gold has an average size of 6 nm with a large deviation of 2 nm; Turkevich also found that some chemicals like citrate quenched and stabilized the gold particles

which then show a uniform size distribution.[10] This surfactant quenching and stabilizing technology has then been used for the research of almost all kinds of NPs, especially for the research on controlled dispersion and assembly of NPs.

Many size-dependent properties of NPs have been studied extensively, such as the surface plasma of Au NPs, photoluminescence of semiconducting NPs, and size-induced metal-insulator transition of metal NPs.[11] However, unlike the well-investigated phase behavior of micro-particles,[12] the thermodynamics of NPs has been an ambiguous topic since the discovery of Faraday's gold sol, probably due to the complexity brought by the use of surfactants in current techniques of manipulating NPs and the strong kinetic effect originated from their small size.

1.3 History and Properties of CNTs

CNTs are an important category of 1-dimensional (1-D) NPs. It was first discovered by Ijima in 1991.[13] CNTs can be viewed as rolled up graphene sheets and categorized as SWCNTs and multi-walled CNTs (MWCNTs) by the number of the graphene sheets in the cylindrical structure. The rolling angle (chirality) determines the electronic properties of SWCNTs, i.e., whether the SWCNTs are semiconducting or metallic. All MWCNTs are metallic because each tube is composed of many layers of different chirality. CNTs possess exceptional mechanical,[14] thermal,[15] and electrical properties.[16] These properties, however, are affected strongly by the dispersion state of CNTs, especially for SWCNTs. Surfactants and functional groups are commonly utilized to disperse SWCNTs. The first observation of individual SWCNTs was reported by Smalley group in 2002.[17] By sonication with surfactants and subsequent ultra-

centrifugation, individual SWCNTs can be collected in the supernatant while most SWCNT bundles remained undispersed.

Individual SWCNTs has an average modulus of 1.8 TPa,[14b] a room temperature thermal conductivity of around 3500 $W \cdot m^{-1}K^{-1}$,[18] and a chirality-dependent electrical conductivity.[16b] Significant improvement of the mechanical and conductive performance has been reported for polymer/SWCNTs composites with low SWCNTs loadings.[19] However, in order to utilize many interesting properties of SWCNTs, a robust method has to be developed to produce individually dispersed SWCNT in large-scale.

1.4 Research Objective and Significance

This dissertation focuses on acquiring individual SWCNTs at large-scale without significant degradation of their electrical and optical properties. The dissertation also carries out characterization of the obtained SWCNTs and establishment of generalized approaches to disperse NPs. The specific objectives include:

i. *Isolation of individual SWCNTs from the nanoplatelets dispersants in aqueous environment, investigation of the optical and morphological characteristics of the debundled SWCNTs, and understanding the corresponding mechanisms.*
ii. *Dispersion of individual SWCNTs in organic solvents.*
iii. *Stabilization and dispersion of surfactant-free 0-D QDs, 1-D nanotubes and 2-D nano-sheets using dielectric-constant-matched solvent, understanding the interaction forces between the NPs and solvent.*

iv. Characterization of the solvent-stabilized NPs and selecting a model NP for investigation of the phase behavior.

The accomplishments made in this dissertation would greatly facilitate large-scale processing of CNTs and should have widespread impact on colloidal science in terms of purification and manipulation of NPs.

1.5 Dissertation Layout

A brief problem statement and introduction on the history and properties of NPs, especially of CNTs, has been outlined in this chapter. A detailed literature review will be given on the dispersion of NPs and CNTs will be given in **Chapter II**, as well as the controlled assembly of NPs. In **Chapter III**, the synthesis and pre-treatment of different NPs will be described and a list of raw materials and equipment utilized will be provided.

A previously established method of dispersing SWCNTs using nanoplatelets will be introduced in **Chapter IV.** The interaction between SWCNTs and nanoplatelets is investigated. An electrostatically controlled method of isolating individually dispersed SWCNTs from the nanoplatelet dispersant is developed. Two mechanisms of separating electrostatically conjugated NPs are studied. The obtained SWCNTs are characterized using various microscopy and spectroscopy tools.

In **Chapter V**, an acid-mediated method of separating SWCNT and the nanoplatelets dispersant is introduced. The surfactant effect is discussed. Examples of applications based on the individually dispersed CNT obtained using the acid-mediated approach are demonstrated.

Chapter VI focuses on the dispersion of purified nanoparticles by minimizing vdW attraction. Three model NPs with different geometries, including the purified SWCNTs obtained in the last two chapters, are used to demonstrate the applicability of the approach.

The phase transitions of a surfactant-free ZnO QD colloid are examined in **Chapter VII**. Monodisperse ZnO QDs are found to form various structures under different ionic strength. Theory of the phase behavior of sphere-like particles is briefly introduced. A phase behavior similar to that of micro-spheres is observed with NPs for the first time. The effect of media ionic strength on the phase transitions of the ZnO QDs is discussed.

In the last chapter (**Chapter VIII**), concluding remarks are given, recommendations for further studies are proposed, and references in this dissertation are documented.

CHAPTER II

LITERATURE REVIEW*

2.1 Controlled Dispersion of NPs

Electrostatic and steric stabilization are the two most common methods to disperse NPs. Particles that are electrostatically stabilized typically have a zeta potential higher than 30 mV or lower than -30 mV.[4] This high zeta potential is usually provided by the hydrophilic surfactants coated on the particle surfaces and the coated NPs can form a stable colloidal dispersion in water, such as the mercaptosuccinic acid-coated Au NPs ($2\mathbf{r}$ = 3.7 nm).[20] Two most commonly used hydrophilic surfactants are CTAB and citrates.[21] Peptide and DNA are also often utilized.[22] A rarer case is when the electrostatic force is originated from the defects of the NPs themselves,[23] However, usually the zeta potential of naturally charged NPs is not high enough to provide long-term stability. Interestingly, most NPs used in this field are Au NPs.

In organic solvents, hydrophilic surfactants are less preferable because of their poor solubility; but NPs can be stabilized through steric or electrosteric repulsion using hydrophobic surfactants. For example, a stable dispersion of monodisperse tri-n-octylphosphine/tri-n-octylphosphine oxide capped CdSe semiconducting nanocrystallites ($2\mathbf{r}$ = 1.5 ~ 10 nm) can be prepared in 1-butanol.[24] A more typical example is oleic-acid

---

*Part of this chapter is reprinted with permission from "Colloidal Crystallization of Surfactant-Free ZnO Quantum Dots" by Xi Zhang, Dazhi Sun, Hung-Jue Sue and Richii Nishimura, 2011. *ChemPhysChem*, 12, 3533-3538, Copyright [2011] by Wiley.

-modified NPs for both semiconducting and metallic NPs.[25] Sometimes, surfactant exchange can render a hydrophilic NP hydrophobic or vice versa.[25b, 26]

Research on dispersion of ligand-free or surfactant-free NPs is still quite limited. Stable dispersion has been achieved for pure silica and silicon particles in ethanol-based solvents with primary particle sizes of about 100 nm.[27] However, in a similar solvent environment, silicon NPs of 5 nm in size will tend to form 40-60 nm agglomerates.[28] ZnO NPs have also been found unstable without presence of stabilizers.[23] Previously, it has been found that the addition of hexane slows the aggregation rate of purified ZnO QDs prepared in methanol.[29] However, no extensive research has been carried out due to poor miscibility between methanol and hexane, and the authors have not provided any in-depth explanation of the mechanism.

2.2 Controlled Assembly of NPs

Assembly of functional nanoscale objects into ordered macro-size materials offers unique opportunities for discovering new physical phenomena and fabricating novel electro-magnetically or electro-optically active devices based on the collective effects of the building blocks incorporated. Recent advances in both bottom-up and top-down technologies have allowed for the fabrication of periodic 1-D and 2-D arrays of nanostructures over a relatively large scale.[22a, 30] However, 3-D ordering of nanoscale objects into macro-scale materials remains a challenge for most nanoparticle (NP) assembly systems. The utilization of surfactants in current NP assembling approach has also compromised definitive understanding of the phase behavior of NP colloids.

Colloidal crystals up to several microns in size from hydrophilic mercaptosuccinic acid-coated Au NPs have been reported to have a hexagonal-close-packed structure.[20] Light-controlled self-assembly of Au NPs with photoactive ligands has led to 3D body-centered cubic (bcc) supracrystals.[31] Recently, a successful approach based on DNA-guided, programmable NP crystallization (bcc and face-centered cubic (fcc)) has been demonstrated to form micron-sized 3D colloidal crystalline domains.[32] However, several key obstacles remain to be overcome before these current approaches can become practical. First, the building blocks are generally limited to DNA-functionalized or ligand-activated metallic NPs. Many active NPs, such as semiconducting QDs and magnetic NPs, have not been successfully utilized due to difficulty in conjugation of NPs and desirable functional surfactants. Second, the colloidal crystal networks formed using DNA-guided approach only exist in solution; if the solvent is removed, the crystalline structural characteristics are lost.[33]

On the other hand, colloidal crystals of ligand-capped QDs in organic solvents can be formed by adjusting the solvent composition, evaporation or diffusion.[34] However, current approaches, as well as those using metallic NPs, often yield crystalline domains limited in micrometer size scale, possibly due to the fact that current NP-based self-assembly techniques usually start from a diluted dispersion of NPs and the sparsely distributed nucleation sites restrict the further growth of larger NP crystals.

2.3 Dispersion of SWCNTs

Exfoliation and dispersion of SWCNTs at individual level is desirable for both fundamental research and industrial applications. However, with few exceptions of

laboratory-scale methods, such as in-situ growth on patterned substrates[35] and in-situ polymer grafting,[36] SWCNTs tend to self-assemble into insoluble bundles or ropes with strong hydrophobicity and significant inter-tube van der Waals interaction (≈ 20 kT for every nanometer of tube overlap).[37] Two main approaches have been used to address these challenges: 1) alter the surface characteristics of SWCNTs by covalent functionalization[38] and 2) modify the direct interaction between SWCNTs and dispersing media with an intermediate small molecule surfactant,[17, 39] polymeric surfactant,[40] DNA molecules,[41] or dispersant particles,[42] i.e., non-covalent approaches. The efficiency of covalent methods in debundling SWCNTs is highly dependent on the reaction condition. Harsh chemical treatment can be extremely effective in interrupting the secondary inter-tube interactions and solubilizing individual nanotubes; a high yield of well-dispersed SWCNTs can be achieved. However, harsh reaction conditions often cause significant deterioration of the physical and electronic properties of the nanotubes.[43] Gebhardt et al.[44] recently developed a mild covalent reaction route to functionalize SWCNTs with carbonyl compounds under modified Birch conditions without significant alteration of the excitonic transition features of the SWCNTs. However, the organometallic reduction approach requires stringent environmental conditions and subsequent centrifugation to remove SWCNT aggregates; and it is unclear whether SWCNTs are indeed dispersed on the individual level. Similar limitations can be found with other mild functionalization methods reported for SWCNTs.[45]

Non-covalent treatment is capable of preserving the intrinsic properties of SWCNTs, but typically requires rigorous mixing and intensive ultra-centrifugation and has low yields, with <10% individual SWCNTs can be recovered by common surfactants.[39] In order to effectively optimize the performance of SWCNT-based devices, scalable processing techniques must be developed which are capable of both exfoliating individual nanotubes without damaging the structure or electronic state of the pristine material and maintaining individual dispersion when transferred to a solvent or material of choice.

2.4 Concluding Remarks

Surfactants and ligand are commonly used to disperse NPs, including CNTs. Currently an in-depth understanding of the dispersion of surfactant-free NPs is absent; the involvement of surfactants also tends to complicate the assembling behavior of the NPs. A model NP that can be dispersed or assembled in a controlled manner without using surfactants is highly desirable.

When using surfactants to obtain individual SWCNTs, the intrinsic physical and electronic properties of CNTs can be maintained. However, the yield of the individually dispersed SWCNTs is usually low, limiting its application in large-scale. Previously, we have found that mildly oxidized SWCNTs can be exfoliated by positively charged ZrP nanoplatelets, without significant structural degradation. The interaction between ZrP and the SWCNTs is likely to be electrostatic. Isolation of the individual SWCNTs from the nanoplatelet dispersant will help explore the full potential of well-dispersed SWCNTs for various academic and industrial applications.

CHAPTER III

MATERIALS AND CHARACTERIZATION

3.1 Materials

Purified HiPco SWCNTs (pristine SWCNTs) and XD-grade SWCNTs were obtained from Carbon Nanotechnologies, Inc. MWCNTs were obtained from Arkema. CNTs used in this dissertation were pre-treated in most cases. ZnO QDs and ZrP nanoplatelets were synthesized using previously reported methods. Details about the pre-treatment of CNTs and the synthesis of ZnO QDs and ZrP nanoplatelets are described below. Listed here are raw materials that are used as received.

i. Acids

Sulphuric acid (H_2SO_4, 95–98%), nitric acid (HNO_3, 68-70%), phosphoric acid (H_3PO_4) and hydrochloric acid (HCl) were purchased from EMD Chemicals.

ii. Salts

Potassium hydroxide (KOH), sodium chloride (NaCl), potassium chloride (KCl), magnesium chloride ($MgCl_2$), calcium chloride ($CaCl_2$), sodium sulfate (Na_2SO_4), magnesium sulfate ($MgSO_4$), lanthanum chloride ($LaCl_3$) and potassium acetate (CH_3COOK)) were purchased from Sigma-Aldrich.

iii. Surfactants

Sodium dodecylsulfate (SDS), sodium dodecylbenzenesulfonate (SDBS), Triton X-100 (TX-100), pluronic F-127, polyvinylpyrrolidone (PVP), cetyltrimethylammonium bromide (CTAB) were purchased from Sigma-Aldrich. Polyvinylalcohol (PVA) was purchased from Fluka. Brij 700 was obtained from Spectrum Chemical Mfg Corp..

iv. Other

All organic solvents are HPLC or ACS grade, purchased from Sigma-Aldrich or VWR. ZrP nanoplatelet precursor zirconyl chloride ($ZrOCl_2 \cdot 8H_2O$) was purchased from Sigma-Aldrich. Tetrabutylammonium hydroxide (TBA^+OH^-, 1 M in water) and ZnO precursor zinc acetate dihydrate ($(CH_3COO)_2Zn \cdot 2H_2O$) were purchased from Fluka. Polyvinylidenefluoride (PVDF) membranes with 0.45 μm pore size were from Millipore.

3.2 Synthesis of ZnO QDs

Colloidal ZnO QDs were prepared by hydralyzing $(CH_3COO)_2Zn \cdot 2H_2O$ in a methanol solution containing KOH.[29] The concentrations of Zn^{2+} and K^+ were 0.04 M and 0.08 M, respectively. The solution mixture was refluxed and stirred at 60 ^oC for 2 hours and then concentrated 10 times at 40 ^oC *via* rotary evaporation. The obtained ZnO sol was then purified to be dispersed in a dielectric-constant-mateched solvent as in Chapter VI, or manipulated to form a ZnO QD ensemble as in Chapter VII.

3.3 Synthesis and Exfoliation of ZrP Nanoplatelets

The ZrP nanoplatelets used in this work, having a lateral dimension of about 100 nm and plate thickness of 7.6 Å, were synthesized by refluxing $ZrOCl_2$ in 3 M H_3PO_4 solution at 100-110 ^oC for 24 hours.[46] The synthesized pristine ZrP was then cleansed with deionized water (DI H_2O). Typically, the delamination and exfoliation of the nanoplatelets was accomplished by sonication with TBA^+OH^- in water with a molar ratio of ZrP:TBA = 1:0.8. The obtained ZrP-TBA conjugate has a chemical formula of $Zr(HPO_4)_{1.2}(TBA^+PO4^-)_{0.8}\cdot nH2O$ ($n \approx 1$).[47]

3.4 Pre-treatment of CNTs and Exfoliation of CNTs using ZrP

The pre-treatment of P-SWCNTs was carried out by oxidizing 100 mg P-SWCNTs in 24 mL concentrated H_2SO_4:HNO_3 mixture (3:1 volume ratio) at room temperature in an ultrasonication bath (Branson 2510) for 3 hours.[42b] After sonication, 76 ml DI H_2O was added and the mixture was sonicated for another hour. Oxidized SWCNTs were isolated under vacuum using a PVDF filter membrane and washed several times with KOH aqueous solution (100 mM) and DI H_2O during filtration to remove residue and intercalated oxyacids thoroughly.[48] Diluted HCl (100 mM) was then used to restore carboxylic groups (-COOH) on SWCNT surface.[49] Afterwards, oxidized SWCNTs (O-SWCNTs) were cleaned with DI H_2O and re-dispersed into an aqueous suspension. Other types of CNTs were treated similarly, except for MWCNTs, which was oxidized in H_2SO_4:HNO_3 mixture for 2 hours instead of 3 hours.

To exfoliate CNTs, aqueous solutions of oxidized CNTs and fully exfoliated ZrP nanoplatelets were directly mixed and sonicated for 30 minutes. The weight ratio of

CNT to ZrP nanoplatelets was set at 1:5. During this step, the SWCNTs are electrostatically bound to the nanoplatelets and are exfoliated to the individual nanotube level.[42b, 50]

3.5 Characterization

TEM micrographs were acquired with a JEOL 2010 high-resolution transmission electron microscope operated at 200 kV. UV-vis or UV-vis-NIR spectra were obtained with a Shimadzu UV-3600 UV-vis-NIR spectrometer, except in Chapter VII, where the UV-vis spectra of ZnO were obtained on a Hitachi U4100 UV-Vis-NIR Spectrophotometer. Energy dispersive X-ray spectroscopy (EDS) analysis was performed on a Quanta 600 field emission scanning electron microscope (SEM). X-ray photoelectron spectroscopy (XPS) analysis was carried out using a Kratos axis ultra-imaging X-ray photoelectron spectrometer. Raman data was obtained on a Horiba Jobin-Yvon LabRam IR system; the sample was excited with a 633-nm laser. Photoluminescence (PL) data was acquired on a PTI QuantaMaster Spectrofluorometer. X-ray diffraction (XRD) patterns and small-angle X-ray scattering (SAXS) patterns were collected on a Bruker D8 Advanced Powder X-ray Diffractometer with Cu-K_α incident radiation (λ = 1.5418 Å) and a BRUKER NANO-STAR Rotating Anode SAXS Instrument (λ = 1.5418 Å), respectively.

CHAPTER IV

ELECTROSTATICALLY CONTROLLED ISOLATION OF DEBUNDLED SWCNTS FROM NANOPLATELET DISPERSANT

4.1 Introduction

We have previously demonstrated that mildly oxidized SWCNT bundles can be fully exfoliated using synthetic charged inorganic nanoplatelets.[42b] In essence, the approach involves electrostatically tethering the slightly oxidized SWCNTs to the surface of positively charged ZrP nanoplatelets. The ZrP aids in the physical separation of the SWCNTs to the individual level by transferring sonication energy to SWCNT bundles. The preserved electronic state and structural integrity of the individual SWCNTs have been demonstrated and the SWCNT-ZrP hybrid has been demonstrated to be highly effective in improving the mechanical and electrical properties of polymers or composites.[42b, 50] To further explore the potentials of the fully debundled SWCNTs, methods have to be developed to isolate the exfoliated SWCNTs from the nanoplatelet dispersant.

In this chapter, the interaction between SWCNTs and ZrP is studied extensively and an effective method is developed to isolate the exfoliated SWCNTs from the nanoplatelets. The isolation of SWCNTs was accomplished by precipitating nanoplatelets with cations and by concurrent usage of appropriate surfactants to stabilize SWCNT. It was found that the precipitation of nanoplatelets induced by monovalent cations was due to ionic screening effect, whereas ion exchange was the main cause for

nanoplatelet aggregation when divalent cations were used. When the above processes are optimized, isolation of pure SWCNTs with yield greater than 90% can be achieved. Effects of ion valency, ion size, reaction time, concentration of SWCNTs and surfactant type for the separation process are discussed. The structure and composition of the exfoliated SWCNTs were characterized using various microscopy and spectroscopy tools. The above exfoliation and separation approach does not noticeably affect electronic state of SWCNTs, thus highly attractive for applications where optimal SWCNT properties are desired. Similar principles may be utilized to selectively retrieve component(s) of interest for other nanoparticle-based hybrid systems.

4.2 Working Principle

The conceptual processing steps to achieve exfoliation and isolation of SWCNTs are present in Figure 4.1. Typically, SWCNTs form entangled bundles after synthesis (Figure 4.1A) and are insoluble in either aqueous or organic solvents. After mild acid treatment, carboxylic groups are introduced preferentially at the tube ends[42b, 51] and become anionic after dissociation in water. The acid treatment does not cause significant damage to SWCNTs as demonstrated later; and the negative surface charges allow the SWCNTs to attach and be wrapped with the positively charge ZrP nanoplatelets (Figure 4.1B). The rigid nanoplatelets concentrate and transfer sonication energy and facilitate the exfoliation of SWCNTs (Figure 4.1C). Our previous work has shown that 30 min bath sonication is sufficient to debundle SWCNTs to the individual level.[42b]

Generally the isolation of SWCNTs is realized by destabilization and precipitation of ZrP through addition of a salt or an acid, and concurrently using an

appropriate surfactant to stabilize SWCNTs from co-precipitating with ZrP (Figure 4.1D, E). Afterwards, ZrP is removed from the system by centrifugation (Figure 4.1F). The acid-mediated method will be discussed in the next chapter. In this chapter, the aggregation of ZrP is induced by diminishing the interaction between pristine ZrP nanoplatelets and the surface functional groups, i.e., the TBA molecules.

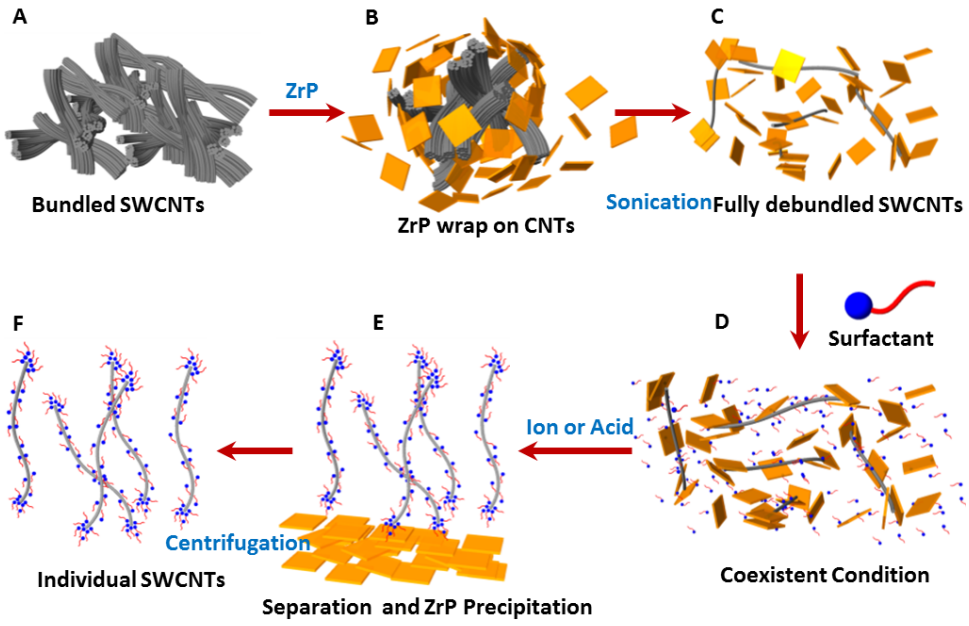

Figure 4.1. Schematic illustration of using ZrP nanoplatelets to exfoliate SWCNTs and subsequent isolation of SWCNTs.

4.3 Theory—The Effect of Counterions on the Surface Charge Sate of ZrP Nanoplatelets

As illustrated in Figure 4.2, the dissociation of phosphate units renders the surface of ZrP nanoplatelets negatively charged and attractive to the cations such as TBA^+. The size differential between the TBA^+ groups and the phosphate units is significant and results in an excess positive charge at the Stern plane,[52] which allows the ZrP-TBA conjugate to bind with anions such as carboxylated CNTs with $–COO^-$ groups on the surface. The Stern layer of bound cations and the diffuse layer of attracted anions are known as electrical double layers (EDLs). Osmotic pressure caused by two approaching EDLs provides a repulsive force which maintains the stability of the nanoplatelets. The thickness of the EDL is highly sensitive to the counterions in the media, and can generally be characterized by Debye length (κ^{-1}). The so-called ionic screening effect implies that upon the addition of counterions (cations in the case of ZrP nanoplatelets), the surface potential (ψ_0) reduces significantly and the EDLs shrinks, causing the destabilization and ultimately the precipitation of the nanoplatelets.

Divalent and trivalent ions are known to have a much stronger ion-screening effect than monovalent ions.[3] Furthermore, with the presence of exchangeable counterions, especially multivalent ions, ion exchange can also occur and lower the surface charge density of ZrP nanoplatelets (σ^*), causing the further drop of ψ_0. The decrease of ψ_0 caused by the ion exchange process can sometimes exceed the ionic screening effect.[3] In the following sections, both mechanisms are discussed with respect to the SWCNT/ZrP separation process.

SWCNTs are inherently insoluble in water and are stabilized by conjugated nanoplatelets solely prior to isolation. Oxidized SWCNTs also have a charged surface sensitive to the presence of counterions. If not stabilized by other dispersants, SWCNTs will co-precipitate with ZrP upon salt addition. To shield the SWCNTs from the counterion effect and prevent co-precipitation, non-ionic surfactant was added prior to cation-induced destabilization of ZrP nanoplatelets.

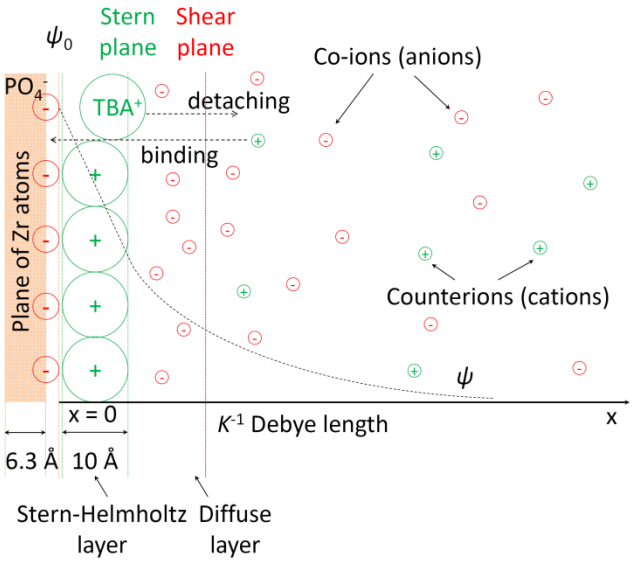

Figure 4.2. Illustration of the surface state of ZrP nanoplatelets, rendered anionic by the dissociation of phosphate units. Electrical double layer is composed of a stern layer of cationic ions and a diffuse layer of anionic ions. The thickness of these double layers can be approximately represented by Debye length. The addition of counterions not only reduces surface potential (ψ_0) *via* ionic screening effect, but also lowers the surface charge density significantly, causing the further drop of ψ_0.

4.4 Experimental

The experiments were carriers out mainly in an aqueous environment of DI H_2O. Once the pre-treated SWCNTs were exfoliated by ZrP, a non-ionic surfactant (e.g. TX-100) was added to the SWCNT/ZrP mixture before the precipitation of ZrP nanoplatelets. The typical concentrations of SWCNTs, ZrP and surfactants in the SWCNT/ZrP/surfactant dispersion are 0.008% (in mass concentration hereafter for the whole dissertation), 0.04%, and 1%, respectively. The isolation of surfactant-stabilized SWCNTs was accomplished by adding salts to induce coagulation and precipitation of the ZrP nanoplatelets. To determine the optimal ion concentration for SWCNT isolation, concentrated aqueous salt solution containing monovalent cations (NaCl, KCl, or Na_2SO_4) was added to reach ion concentrations of 5, 10, 15, 20, 25, 30, 35, 40, 60 and 90 mM. Salt of divalent cations ($MgCl_2$, $CaCl_2$ or $MgSO_4$) was also used at concentrations of 0.1, 0.2, 0.3, 0.4, 0.5, 0.6, 0.7, 0.8, 1.0 and 2.0 mM.

The SWCNT/ZrP/surfactant mixture was sonicated for 30 minutes after salt addition and left for a controlled period of time (Δt) to allow ZrP nanoplatelets to precipitate. Surfactant-stabilized SWCNTs were retrieved from the supernatant after low speed centrifugation (3,400 g) for 5 minutes. The SWCNT yield, i.e., the remaining quantity of debundled SWCNTs in the supernatant after ZrP removal, was determined through absorption spectroscopy in dispersion state. The separation efficiency, i.e., the relative quantity of ZrP nanoplatelets removed from the SWCNT/ZrP/surfactant mixture, was quantified by examining the SWCNT product in solid state after surfactant and ion removal, using EDS and XPS. To evaluate separation efficiency, SWCNTs were

detached from the surfactant by adding excess ions or nonpolar solvents such as acetone to the SWCNT-enriched supernatant to induce SWCNT agglomeration. The aggregated SWCNTs were then rinsed to remove ion and surfactant residue and dispersed in aqueous solution. This process was repeated 3 or 4 times to completely remove the surfactant. Afterwards, SWCNTs were transferred on an aluminum stub or a carbon tape for EDS or XPS analysis, respectively. For TEM observation, the cleansed SWCNTs were re-dispersed in a mixture of ethanol and hexane with a volume ratio of about 1 to 0.9. The reason that this solvent mixture was chosen will be explained in Chapter VI.

4.5 Results and Analysis

4.5.1 Spectroscopic Characterization

Surface oxidation of CNTs in strongly oxidative acids is a common method to introduce carboxylic groups and negative charges on the CNT surface. Unlike similar work done at elevated temperature for long periods of time,[48, 51, 53] the oxidative treatment of SWCNTs in this work was carried out at room temperature for a relatively short time period. This allows adequate negative charges to be imparted for SWCNTs to bind to the positively-charged ZrP nanoplatelets without causing noticeable structural degradation. Raman spectroscopy was used to characterize the damage state of HiPco SWCNTs after different levels of treatment. A typical Raman spectrum of SWCNTs has three relatively intense frequency bands: the symmetric radial breathing mode (RBM, 160-280 cm^{-1}), the tangential C-C stretching mode (G-band, 1460-1660 cm^{-1}) and the so-called D-band (1200-1400 cm^{-1}) which is activated by the presence of in-plane defects in

the sp^2 hybridized carbons.[54] The intensity ratio between D band and G band (D/G ratio) is commonly used to quantify the structural integrity of SWCNTs. As shown in Figure 4.3A-C, the D/G ratio is 0.05 for pristine HiPco SWCNTs (black line) and increases slightly to 0.07 after acid treatment (red line). After mixing and sonication with ZrP nanoplatelets, the D/G ratio of SWCNT/ZrP hybrid (blue line) increases to 0.13, along with 8 cm^{-1} blue shifts in both G-band and D-band, a less noticeable blue shift (3 cm^{-1}) in the RBM region, and broadening of G-band. The increase in D/G ratio and G-band broadening are generally caused by either physical cutting or chemical bonding. The XPS spectra in Figure 4.3D show that the C 1s peak of the SWCNT/ZrP hybrid (blue line) is significantly blue-shifted (2 eV in binding energy) compared with the C 1s peak of pre-treated SWCNTs (red line), suggesting strong electronic coupling between SWCNTs and ZrP. Moreover, after complete ZrP removal, the change of C 1s binding energy is recovered; the D-band intensity and G-band width in Raman spectra reduces to the same level as pre-treated SWCNTs (Figure 4.3A-D, green line). Previously, we have also shown that there is no change in SWCNT length distribution during the exfoliation process.[42b] Therefore, our results strongly indicate that the exfoliation process does not affect the physical or chemical structure of SWCNTs.

Figure 4.3. (A) Raman spectra of pristine SWCNTs (black line), pre-treated SWCNTs (red line), SWCNT/ZrP hybrid (blue line) and SWCNTs after ZrP removal (green line), normalized to G-band intensity, vertically offset by 1 for clarity. (B) Magnified area of D-band (offset by 0.1) and (C) RBM region (offset by 0.2). (D) XPS spectra of pre-treated SWCNTs (red line), SWCNT/ZrP conjugate (blue line) and SWCNTs after ZrP removal (green line). (E) UV-vis-NIR spectra of 0.004% pristine SWCNTs (black lines) and pre-treated SWCNTs (red lines) suspended by TX-100 (dark lines) and SDBS (light lines), vertically offset for clarity. (F) UV-vis-NIR spectra of aqueous solution of pre-treated SWCNTs (red line), SWCNT/ZrP (blue line), SWCNT- and surfactant-enriched supernatant after ZrP removal (dark green line) and SWCNTs re-dispersed in 1 % PVP (pink line). Inset: absorption spectra in UV region showing the intrinsic absorption of grapheme structure of pre-treated SWCNTs and SWCNT/ZrP hybrid, prominent absorption of surfactants in the SWCNT-enriched supernatant and the significantly reduced absorption of surfactants after 1 cycle of precipitation and re-dispersion of SWCNTs (green line).

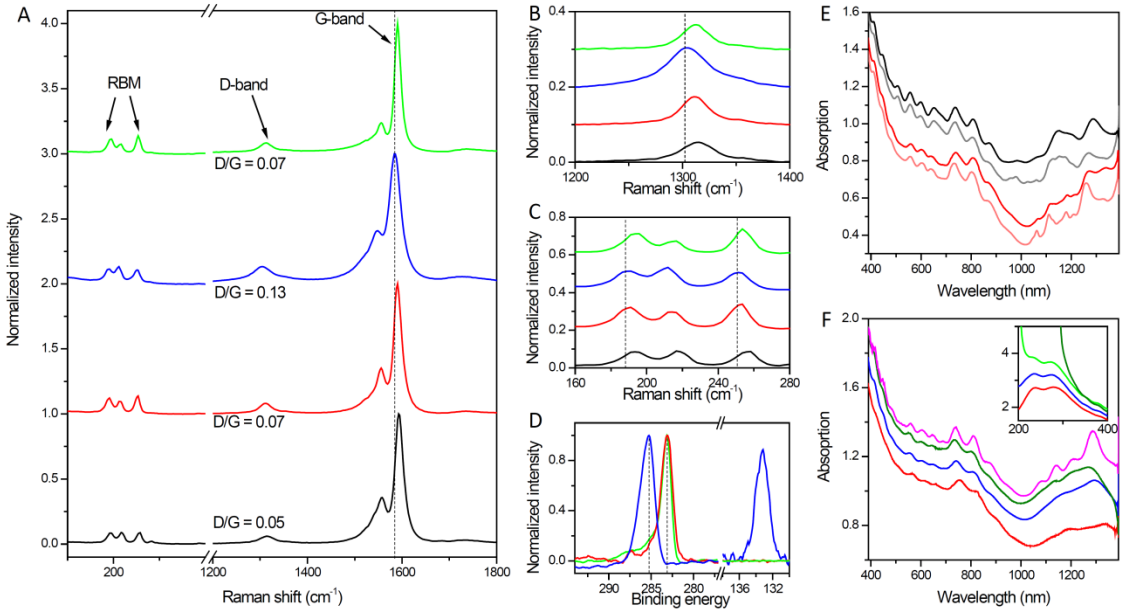

Furthermore, the XPS and Raman results indicate that while the interaction between SWCNTs and ZrP processes a certain level of electronic coupling, shown by the transient increase in D-band intensity and blue shift of C 1s binding energy; reversible electrostatic interaction predominates, as evidenced by the recovery of D/G ratios and C 1s binding energy upon SWCNT/ZrP separation. By tuning the ionic strength of the medium, the electrostatic interaction can be perturbed and SWCNTs and ZrPs can be isolated from each other.

The UV-vis-NIR absorption spectra of pristine SWCNTs (black lines) and pre-treated SWCNTs (red lines) dispersed in aqueous solutions with TX-100 (dark lines) and SDBS (light lines) are shown in Figure 4.3E. The mass concentration of SWCNTs and surfactant is 0.004% and 0.5%, respectively. Each mixture was sonicated for 30 minutes prior to analysis. The first van Hove transition peaks in the NIR region (850-1600 nm) of the absorption spectra is related to the direct band gap absorption of SWCNTs and can

therefore be used to characterize structural integrity and aggregation state.[17, 55] For example, heavy side-wall functionalization causes a complete loss of van Hove transitions.[56] The van Hove transitions of pre-treated SWCNTs is not deteriorated relative to the pristine SWCNTs and appears more de-convoluted in the NIR region. This evidence suggests that the electronic structure of the SWCNTs is well preserved during acid treatment. It also implies that the SWCNT surface becomes slightly more hydrophilic and exhibits better interaction with the aqueous environment. Compared with SDBS, TX-100 is a poor dispersant for HiPco SWCNTs,[57] as seen from the less distinct SWCNT absorption peaks in NIR region. However, the purpose of using TX-100 in our work is not to exfoliate SWCNT bundles but to stabilize the already exfoliated SWCNTs. TX-100 functions well in this aspect as will be shown later.

Both Raman and UV-vis-NIR spectra indicate that the structural difference between pristine and pre-treated SWCNTs is minor; however, the mild damage caused by acid treatment plays an important role in SWCNT exfoliation. When mixed with ZrP at a mass ratio of SWCNT:ZrP = 1:5 in aqueous solution, pre-treated SWCNTs become dispersed and stabilized after 30 minutes sonication, while pristine SWCNTs remain insoluble and particulate under the same treatment. XPS shows that the oxygen content in SWCNTs increases from about 12% to 15% and that the ratio between COO^- and C-O increased from 0.22 to 0.45 during the acid treatment. This indicates that the surface damage caused by acid treatment is mainly due to the conversion from C-O to COO^-, which occurs preferentially at the tube ends.[51] As a result of carboxylation, negative charges imparted on the SWCNT surface render it attractive to positively-charged ZrP

nanoplatelets which are then able to efficiently transfer sonication energy and result in physical debundling of SWCNTs to the individual level.[42b]

UV-vis-NIR spectra of aqueous solution of pre-treated SWCNTs alone, SWCNT/ZrP hybrid after sonication, SWCNT-enriched supernatant after ZrP removal and the re-dispersed SWCNT after isolation from the supernatant are shown in Figure 4.3F. The SWCNT/ZrP mixture (blue line) exhibits a noticeable absorption in van Hove transition range while pre-treated SWCNT alone (red line) exhibits little. However, few de-convoluted peaks are detected in the NIR region which may be due to the presence of highly-charged nanoplatelets interfering with the band-gap absorption of SWCNTs. When TX-100 is used to stabilize SWCNTs, the SWCNT-enriched supernatant (dark green line) exhibits a similar broad absorption in the NIR region after centrifugation even though ZrP is no longer present. This is probably because TX-100 is a poor dispersant, but could also be due to the added ions that suppress the absorption of certain species of HiPco SWCNTs.[58] After precipitation, cleaning, and re-dispersion in a aqueous solution containing 1 % PVP, which has been reported to have robust association with HiPco SWCNTs,[40c] the recovered SWCNTs (pink line) exhibit distinct absorption peaks in the NIR region with significantly enhanced intensity. This indicates the presence of a large amount of individually dispersed SWCNTs.

UV absorption (200-400 nm) of the samples is shown in the inset of Figure 4.3F. The intrinsic absorption of the graphene structure is clearly observed for both pre-treated SWCNTs and the SWCNT/ZrP hybrids. The UV span of the absorption spectrum is not typically shown for surfactant-suspended SWCNT prepared by sonication and

centrifugation because most surfactants have a dominant absorption in this region. Dialysis is typically used to remove or replace surfactants from CNTs.[59] In this study, detachment of SWCNTs from surfactants was achieved by first precipitating the SWCNTs, rinsing to remove ions and surfactants, then re-dispersion by sonication. We notice that the surfactant absorption in the UV span is substantially reduced and that the SWCNT adsorption reappears after only one cycle of precipitation and re-dispersion (green line). Thus, surfactants and ions can be efficiently removed by the process and the temporal aggregation status does not affect its individual dispersion state once the precipitated sample is re-dispersed. Complete surfactant removal allows the transfer of purified SWCNTs into various media and is particularly useful for quantification of the separation efficiency using EDS because the carbon signal from surfactants would otherwise overwhelm that of SWCNTs.

4.5.2 Microscopy Observation

From literature, enhanced absorption in NIR region does not preclude the possible presence of small SWCNT bundles or dimers.[17, 57] To rule out this possibility, direct microscopy observation is needed. TEM micrographs of individually dispersed SWCNTs are shown in Figure 4.4. The dark areas in Figure 4.4A are out-of-focus ZrP nanoplatelets in the SWCNT/ZrP hybrid. The SWCNTs appear as individual and straightened by the nanoplatelets. Figure 4.4B shows isolated SWCNTs without presence of any ZrP or residual surfactant observed and the SWCNT appear more flexible than those in the hybrid system. At a higher magnification (Figure 4.4C), the diameters of well distinguished SWCNTs were measured and range from 0.9 nm to 1.2

nm, which is in good agreement with the diameter of individual HiPco SWCNTs.[60] The dark dots in the image are metal catalyst residue, typically present even in purified HiPco SWCNTs. The conventional homogenization and ultra-centrifugation method is efficient at removing metal residue along with large SWCNT bundles, but the yield of individual SWCNTs with this method is very low (< 10%).[39] The objective of this work has been to obtain substantially higher yield of individual SWCNTs without degrading their electronic properties. Room temperature acid treatment prior to SWCNT exfoliation is not effective at removing the metal catalyst, which suggests the metal particles are likely trapped within SWCNT bundles and do not react with acids. A post-exfoliation purification should enable further removal of exposed metal

EDS element maps generated with low magnification SEM are shown in Figure 4.4D and 4.4E. The mapping was performed on 1.3 mm x 2 mm sections to represent the overall chemical composition of the samples. The SWCNT/ZrP hybrid contains a large quantity of phosphorus (green dot), but almost no phosphorus was observed for the isolated SWCNTs.

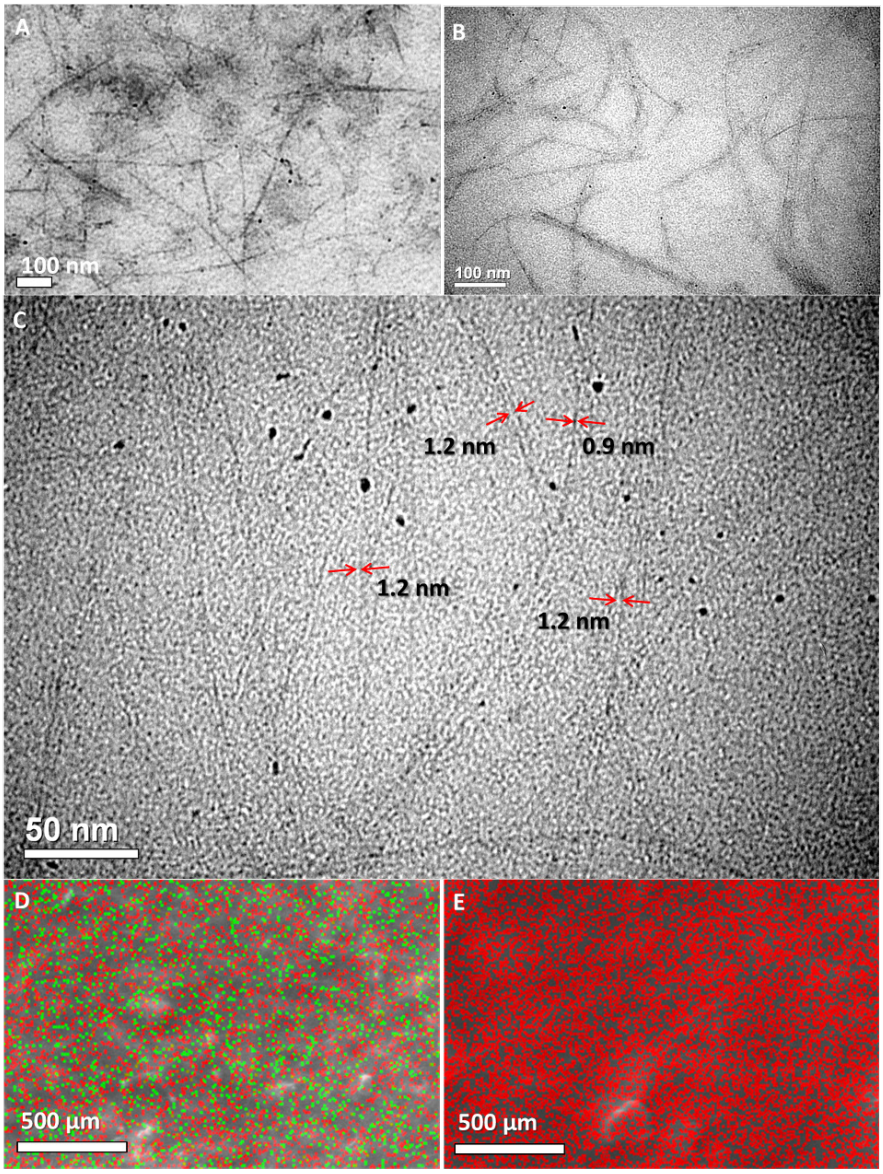

Figure 4.4. (A-C) TEM micrographs of (A) SWCNT/ZrP hybrid, (B) SWCNTs isolated from SWCNT/ZrP/TX-100 mixture and (C) isolated SWCNTs with a diameter from 0.9 to 1.2 nm. (D-E) Element maps of (D) SWCNT/ZrP hybrid and (E) SWCNTs isolated from SWCNT/ZrP/TX-100 mixture. The green dots represent phosphorus, the red dots are carbon and the gray background is aluminum substrate.

4.5.3 SWCNT Yield and Separation Efficiency

i. Dependence on ion species, concentration, size and Δt

Samples were prepared to determine the conditions necessary to achieve maximum yield of individual SWCNTs. The effect of salt concentration ([Salt]) is shown in Figure 4.5. When using NaCl to induce precipitation of ZrP in a SWCNT/ZrP/TX-100 mixture (0.008% SWCNT, 0.04% ZrP and 1% TX-100 by mass), separation efficiency quantified using EDS shows that no separation would occur until [NaCl] reaches 15 mM (Figure 4.5A, empty blue circles). Above this concentration, the separation efficiency increases substantially and approaches 100% at [NaCl] = 25 mM. The separation efficiency calculated from XPS is also provided (open squares) and shows slight deviation from EDS results, but with the same trend of improvement in separation efficiency between [NaCl] = 15 mM and 25 mM. Therefore, the NaCl concentration at the separation onset ($[NaCl]_{ost}$) is 15 mM but the minimum concentration of NaCl required to completely remove ZrP ($[NaCl]_{min}$) is 25 mM. XPS also indicates that there is negligible nitrogen present in the ZrP-enriched precipitates, which demonstrates that the salt addition efficiently weakens the electrostatic bonding between TBA^+ and ZrP. TBA^+ groups which diffuse into the SWCNT-enriched supernatant can be later removed, along with other ions and surfactants.

The yield of isolated SWCNTs in the supernatant was determined by measuring SWCNT concentration ([SWCNT]) based on the Beer–Lambert law for homogenous dispersion, $A = blc$ (A: absorption intensity; b: constant; l: light path length; c: solute concentration), which indicates a linear dependence of absorption on [SWCNT] (see

APPENDIX A). The yield of isolated SWCNTs as a function of [NaCl] is shown in Figure 4.5A (solid black circles). Prior to $[NaCl]_{ost}$, the yield is 100% and begins to drop gradually as [NaCl] increases. At $[NaCl]_{min}$ (25 mM) and until [NaCl] exceeds 40 mM, SWCNT yield is 91±2%. This optimal condition is encircled by the green rectangle in Figure 4.5A. With higher salt content, the yield rapidly decreases to only 67% at [NaCl] = 60 mM, 7% at [NaCl]= 90mM, and appears to approach zero.

The use of $NaSO_4$ exhibits a similar trend, suggesting that the precipitation of ZrP relies on cations but not anions. When $MgCl_2$ was used, we found that $[MgCl_2]_{ost}$ equals to 0.4 mM and $[MgCl_2]_{min}$ equals to 0.6 mM, much lower values than using NaCl, as shown in Figure 4.5B. However, the use of $MgCl_2$ gives a narrower window (0.6-0.7 mM) for optimized separation and yield of 93±1% within, which is slightly higher than that for NaCl. SWCNT yield dropped to 80% $[MgCl_2]$ = 0.8 mM and 8% at $[MgCl_2]$ = 2 mM. $MgSO_4$ behaves in a similar manner as $MgCl_2$. Options for trivalent cations are limited because most of them either hydrolyze or form complexes in the neutral aqueous solution (pH ~ 7). Lanthanum(III) (La^{3+}) and erbium(III) (Er^{3+}) have been used to manipulate the dispersion state of proteins and SWCNTs,[58, 61] but are uneconomic and difficult to be adapted in our work. Preliminary results indicate that the optimal condition to separate SWCNT and ZrP using trivalent cations is somewhere between salt concentrations of 0.3 and 0.4 mM. The exact range, however, is difficulty to determine because of their high valence charges.

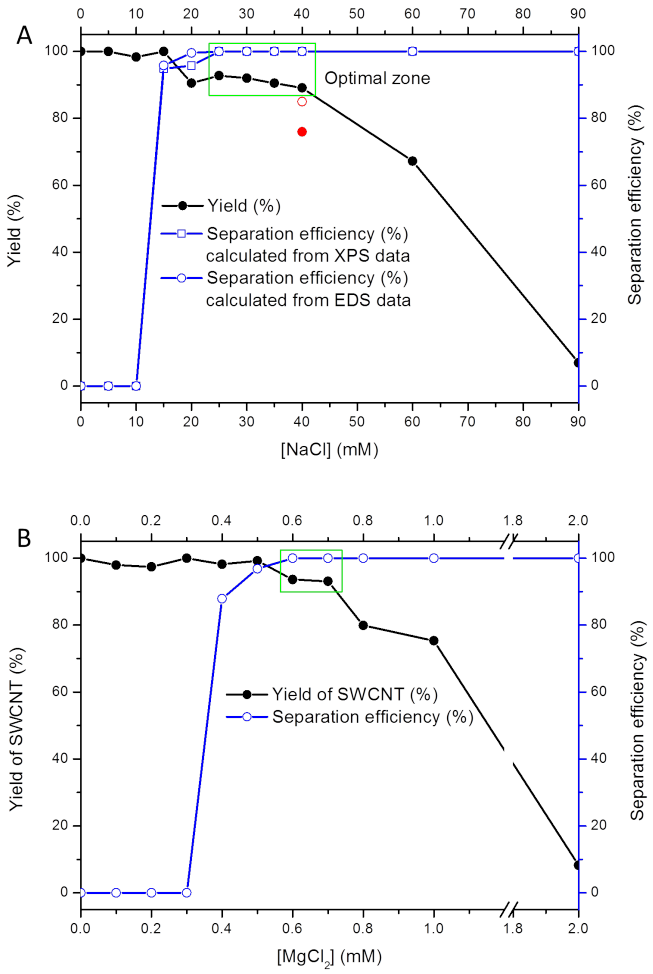

Figure 4.5 (A) SWCNT yield and separation efficiency versus [NaCl], Δt = 20 hr and (B) [$MgCl_2$], Δt = 24 hr. Optimal condition for 100% separation efficiency and maximum SWCNT yield squared by the green rectangle. Empty red circle: separation efficiency at Δt = 10 min. Solid red circle: SWCNT yield at Δt = 72 hr.

KCl and $CaCl_2$ have also been used to separate SWCNT and ZrP. The absorption onset and complete separation occur at about the same concentration as chlorides of their

smaller group elements. However, the SWCNT yield is lower as summarized in Table 4.1.

Table 4.1. Ion concentration at separation onset and corresponding κ^{-1}. Minimum ion concentration required for a complete separation and corresponding SWCNT yield. Conditions listed for a SWCNT/ZrP/TX-100 mixture containing 0.008 % SWCNTs, 0.04% ZrP and 1% TX-100 by mass.

At the separation onset				
	NaCl[a]	KCl[b]	$MgCl_2$[c]	$CaCl_2$[d]
$[Salt]_{ost}$ (mM)	15	15	0.4	0.4
κ^{-1} (nm)	2.4	2.4	6.4	6.4
Dependent on [ZrP]?	No	No	Yes	Yes
At the minimum ion concentration for a complete separation				
	NaCl[a]	KCl[b]	$MgCl_2$[c]	$CaCl_2$[d]
$[Salt]_{min}$ (mM)	25	25	0.6	0.6
SWCNT yield (%)	93	83	94	88
Dependent on [ZrP]?	No	No	Yes	Yes

[a] Δt = 20 hr, [b] Δt = 10 min, [c] Δt = 24 hr, [d] Δt = 2 hr.

The time between sonication after salt addition and centrifugation (Δt) was found to be important for both SWCNT yield and separation efficiency. As shown in Figure 4.5A, when centrifugation was performed immediately after sonication, only 85% ZrP precipitated from the mixture (empty red circle). When centrifugation was performed 72

hours later, yield was reduced to less than 80% (solid red circle). The optimal timing to achieve both high yield and complete separation of SWCNT and ZrP exhibits dependence on cation size, and has been identified as Δt =16~20 hr for NaCl, Δt = 20~24 hr $MgCl_2$, Δt = 2 hr for $CaCl_2$ and Δt = 0 for KCl if samples were left undisturbed at room temperature. Bigger cations seem to cause the precipitation of both SWCNT and ZrP faster than smaller cations, possibly because that they exhibit faster loading rate in ion exchange process with ZrP nanoplatelets[62] and stronger dehydration effect that affect the solubility and stability of non-ionic surfactants.[63]

ii. Dependence on ion valence

Table 4.1 lists the separation conditions, corresponding κ^{-1} at the separation onset, and SWCNT yield at complete separation for a SWCNT/ZrP/TX-100 mixture (0.008% SWCNT, 0.04% ZrP and 1% TX-100 by mass). The calculation of κ^{-1} was done by noting the concentration of 1.1 mM added TBA^+OH^- during ZrP exfoliation. Assuming a constant surface charge density of ZrP nanoplatelets (σ^* = constant), κ^{-1} at the separation onset should be the same for all types of salts and independent on [ZrP], because surface potential ψ_0 is equal to $\sigma^* \cdot \kappa^{-1}/\varepsilon$, where ε is the permittivity of the solution, according to the diffuse double layer model.[2] For brevity, we use the Debye-Huckel approximation for the diffuse double layer model, which gives $\psi_0 = \sigma^* \cdot \kappa^{-1}/\varepsilon$, where κ^{-1} is determined by ε, temperautre, and type and concentration of the electrolyte. The approximation is applicable when $\psi_0 \leq 25.7$ mV.[2] Assuming all dissociated phsphate units are paired with TBA^+, σ^* is estimated to be $2.04 \cdot 10^{-2}$ $C \cdot m^{-2}$. At $[NaCl]_{ost}$ = 15 mM, κ^{-1} = 2.4 nm, $\varepsilon = \varepsilon_r \varepsilon_0 = 6.96 \cdot 10^{-10}$ $C \cdot V^{-1} \cdot m^{-1}$ for water at 25 ^oC, and ψ_0 is

calculated to be 70 mV. This, however, does not invalidate the claims in this work since the Gouy-Chapman theory for highly charged particles invovles the same parameters as the Debye-Huckel approximation and it also implies that ψ_0 is independent of particle density.[2]

However, compared with monovalent cations, divalent cations induce precipitation of ZrP at a much lower concentration and larger κ^{-1} (6.4 nm). The dissimilarity in magnitude of κ^{-1} between the cases using monovalent or divalent cations suggests that divalent cations do not induce ZrP aggregation through the ionic screening effect. Considering that the presence of TBA^+OH^- alone should reduce κ^{-1} from 964 nm for pure water to 9.3 nm, the ionic screening effect caused by divalent cations at the separation onset (κ^{-1} = 6.4 nm) and complete separation (κ^{-1} = 5.7 nm) is likely to be trivial.

Furthermore, concentration of divalent cations needed to cause the precipitation of ZrP nanoplatelets is within the same scale as that of the ZrP (1.3 mM) and exhibits a dependence on the concentration of ZrP. ZrP nanoplatelets are known to be important ion-exchanging materials which allow both monovalent and divalent cations to replace hydrogen ions in the phosphate units at appropriated temperature and pH value.[62] However, the tendency of multivalent ions to bind to the nanoplatelet is much stronger than monovalent ions even at a much lower concentration and this process can significantly reduce σ^* ($\sigma^* \neq$ constant) that the charged nanoplatelet surfaces can be neutralized or the charge state is even reversed.[3] Unlike the ionic screening effect, ion exchange process also relies on the concentration of ZrP nanoplatelets: the higher the

ZrP concentration, the more counterions needed to reduce σ^*. The dependence of ion concentration on ZrP concentration at separation onset and complete separation has been observed for divalent cations, but not for monovalent cations. This indicates that divalent ions mainly act to induce ZrP aggregation through ion exchange, while monovalent ions work primarily through ionic screen effect.

iii. Dependence of SWCNT yield on [SWCNT] and [ZrP]

The SWCNT yield as a function of [SWCNT] is shown in Figure 4.6. The mass ratio of SWCNT to ZrP was kept at 1:5 and surfactant (TX-100) concentration at 1%. At concentration of 25mM of both NaCl and KCl, the yield monotonically decreases as [SWCNT] increases and reduces drastically when [SWCNT] exceeds 0.06% (Figure 4.6A. The behavior for $MgCl_2$ is slightly different. As mentioned previously, $MgCl_2$ precipitates ZrP principally through an ion-exchange process in which higher concentrations of SWCNT and ZrP require a greater amount of $MgCl_2$ to facilitate complete separation. It is difficult to explicitly determine the contribution of $MgCl_2$ with regard to either ionic screening or ion exchange effect because of the complexity of the system. Therefore, we increased the concentration of [$MgCl_2$] linearly with [SWCNT] to ensure complete separation. The SWCNT yield monotonically decreases with increasing concentration of SWCNT without leveling off (Figure 4.6B). It appears that monovalent cations provide the advantage of high batch yield for concentrated samples; whereas divalent cations may be preferable for very dilute systems. However, the concentration of SWCNTs must be maintained below 0.06% even with monovalent cations to avoid significant SWCNT loss.

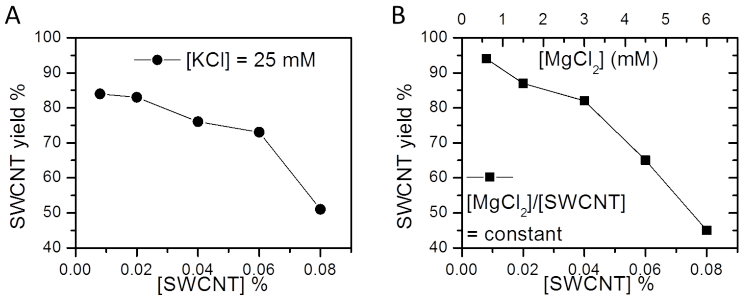

Figure 4.6 SWCNT yield versus [SWCNT]. (A) [KCl] = 25 mM, (B) [$MgCl_2$] is increased linearly as [SWCNT] increases.

iv. Dependence on surfactant type

To isolate SWCNTs from ZrP, the ion/surfactant combination is limited to non-ionic surfactants because most ionic surfactants, such as SDS, SDBS and CTAB, cannot selectively stabilize SWCNTs in the ionic environment. We have developed a method to isolate SWCNTs from ZrP using anionic surfactant which will be introduced in the next Chapter. The method introduced in this chapter is applicable to many other non-ionic surfactants. Besides TX-100, surfactants that have been utilized to assist SWCNT/ZrP separation include PVA, PVP, Brij 700 and pluronic F-127; the latter two have been used to yeild most concentrated dispersion of SWCNTs through conventional homogenization and ultracentrifugation method.[39] Solutions of 0.008% SWCNT, 0.04% ZrP and 1% surfactants have been prepared and 0.6 mM $MgCl_2$ was used to precipitate ZrP. The resultant SWCNT yield is listed in Table 4.2. All surfactants lead to SWCNT yield at around 90%. Especially, Brij 700 and pluronic F-127 stabilize about 96% SWCNT during precipitation of ZrP.

Table 4.2 SWCNT yields with usage of different surfactants.

Surfactant	TX-100	Brij 700	Pluronic F-127	PVA	PVP
SWCNT yield (%)	94	96	96	89	87

[SWCNT] = 0.008%, [ZrP] = 0.04%, [surfactant] = 1%, [$MgCl_2$] = 0.6 mM.

4.6 Conclusions

An efficient method has been developed to isolate HiPco SWCNT from the ZrP nanoplatelet dispersants which were previously utilized to fully exfoliate SWCNTs. Debundled SWCNTs without significant structural degradation have been produced at high yield. The separation between SWCNT and ZrP was achieved by precipitating ZrP through salt addition while SWCNTs were stabilized with non-ionic surfactants. Over 90% of SWCNT can be retrieved from the supernatant with 100% of ZrP removal. Cations are found to be responsible for the precipitation of ZrP. Monovalent cations induce ZrP precipitation through ionic screening, whereas divalent cations primarily work through ion exchange. SWCNTs can be isolated from supernatant without re-bundling or other loss in exfoliation state. XPS, UV-Vis-NIR, Raman spectroscopy and electron microscopy have been used to characterize the SWCNTs and show that the structural and electronic integrity is well preserved during the exfoliation and separation process. The current work has been extended to many other types of SWCNT and MWCNT. In the next Chapter, an acid-mediated isolation route is introduced which allows ionic surfactants to be utilized for CNT stabilization and CNT functionalization after CNT-ZrP separation.

CHAPTER V

ACID-MEDIATED ISOLATION OF DEBUNDLED SWCNTS FROM ELECTROSTATICALLY TETHERED NANOPLATELET DISPERSANT

5.1 Introduction

In the previous chapter, the isolation of individual SWCNTs from the electrostatically tethered nanoplatelet dispersants is accomplished by adjusting the ionic strength of the aqueous environment. This ionic isolation approach is rather limited since it requires the use of non-ionic surfactants to stabilize SWCNTs and salts to coagulate and precipitate the ZrP nanoplatelets. In this work, a superior acid-mediated approach is used to separate SWCNTs and nanoplatelets by means of a strong acid. Using this method, both non-ionic and anionic surfactants can be chosen to stabilize exfoliated SWCNTs in aqueous solution. A broader selection of surfactants allows the well-dispersed CNTs to be stabilized in more varieties of solvents and polymer matrices. We have also successfully used this method to study the electrical percolation behavior of highly-exfoliated SWCNTs formed in a 2-D network.[64] The acid approach can be optimized to recover over 80 % of individually dispersed SWCNTs from the original pristine, bundled SWCNTs. UV-vis-NIR spectroscopy and TEM were carried out to confirm the exfoliation state of the SWCNTs. The acid purification approach is highly versatile and allows for subsequent functionalization of individual CNTs in the aqueous environment. The implication of the current finding for production of well-dispersed

CNTs in both solvents and polymer matrices in large scale for various applications is discussed.

5.2 Working Principle

As shown in Figure 5.1, pristine ZrP nanoplatelets form a white slurry solution when dispersed in water. The nanoplatelets stack together to form tactoids (Figure 5.1A). Once exfoliated by TBA, the solution becomes transparent with a slight bluish tint (Figure 5.1B). The conjugated TBA-ZrP possesses excess positive charges due to the size differential between the phosphate units and TBA groups.[42b, 52] Therefore, TBA-ZrP can bind to carboxylated SWCNTs and facilitate SWCNT exfoliation.

In Chapter IV, the binding between ZrP nanoplatelets and TBA groups can be viewed as an electrostatic interaction between anionic and cationic particles, which can be interrupted with extra electrolytes. The interaction can also be considered as a reversible reaction between a weak acid (HPO_4^{2-} units on the surface of ZrP nanoplatelets, acid dissociation constant (p*K*a) equals 12.3)[65] and a strong base TBA^+OH^-. Consequently, a small amount of strong acid, such as HCl (100% dissociated in water, p*K*a = -7), can easily cause destabilization and coagulation of ZrP. Indeed, visible ZrP aggregation is observed within 10 minutes using only 0.5 mM of HCl in a 0.04% exfoliated ZrP dispersion. In contrast, >10 mM of monovalent metal cations is required when the ZrP aggregation is induced by salts. The low concentration of ions in the acid-mediated approach allows both non-ionic and ionic surfactants to be used to retrieve the CNTs. XPS analysis on the destabilized ZrP aggregate (washed with DI H_2O) shows a total absence of nitrogen, which indicates that nearly all TBA molecules

are detached by the added acid. Short-time, low-speed centrifugation can be used to accelerate the precipitation of ZrP nanoplatelets and avoid significant CNT loss that can occur after several hours of ultracentrifugation. Interestingly, the destabilized ZrP nanoplatelets assemble into a transparent gel after centrifugation (Figure 5.1C) and can be easily removed from the solution by decanting the supernatant.

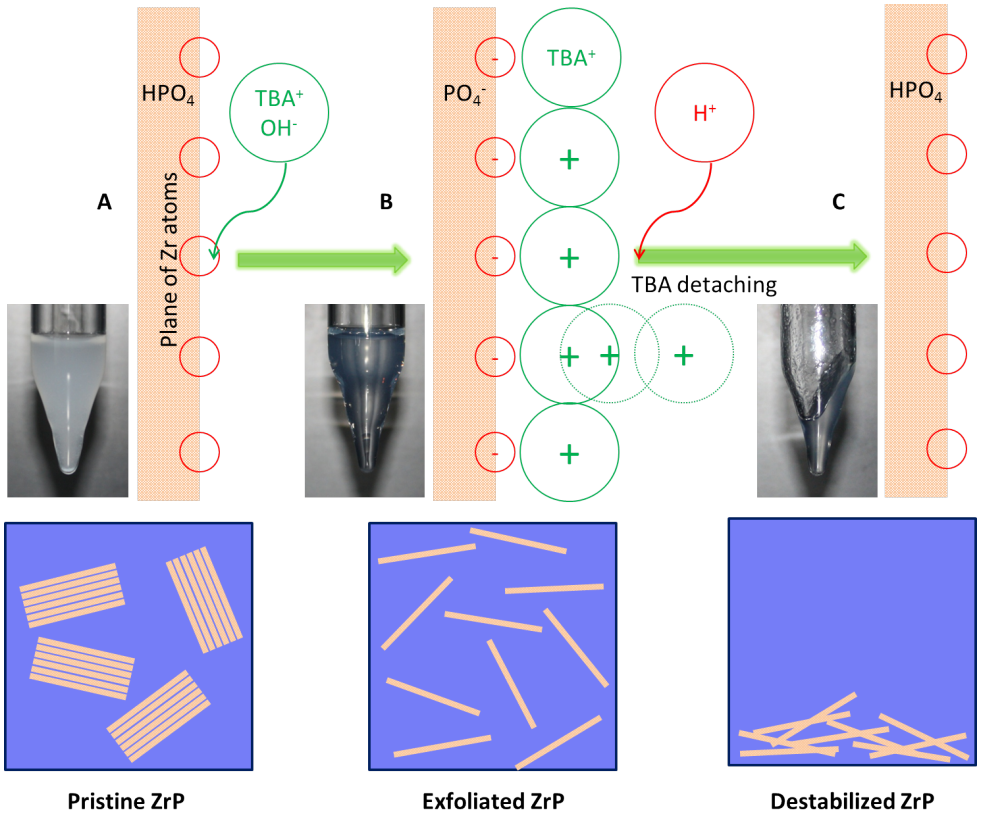

Figure 5.1. The surface functionality and dispersion state of (A) pristine ZrP nanoplatelets, (B) ZrP exfoliated by TBA, and (C) nanoplatelets destabilized by acid.

5.3 Experimental

Once the pre-treated SWCNTs were exfoliated by ZrP, an anionic surfactant, such as SDS and SDBS, or a non-ionic surfactant, like TX-100, was then added to the SWCNT/ZrP aqueous solution and the mixture was homogenized by stirring or sonication. The typical concentrations of SWCNT, ZrP and surfactants in the SWCNT/ZrP/surfactant dispersion are 0.008%, 0.04%, and 1%, respectively. After addition of the surfactant, diluted HCl solution (100 mM) was used to induce coagulation and precipitation of ZrP nanoplatelets. To determine the optimal concentration of acid to achieve maximum SWCNT yield and separation efficiency, a concentrated aqueous solution of HCl was added while stirring to reach H^+ concentration ($[H^+]$) of 0.50, 0.75, 1.00 and 1.25 mM for a SWCNT/ZrP/SDS dispersion and 1.50, 1.75, 2.00 and 2.50 mM for a SWCNT/ZrP/TX-100 dispersion.

The SWCNT/ZrP/surfactant mixture was stirred overnight and then centrifuged at 16,800 G for 10 min. The SWCNT yield was determined *via* absorption spectroscopy (APPENDIX A). To evaluate the separation efficiency, SWCNTs were further isolated from the surfactant by adding excess ions (when TX-100 was used) or nonpolar solvent such as acetone (when SDS was used) to the SWCNT-enriched supernatant to induce SWCNT agglomeration. The aggregated SWCNTs were washed and re-dispersed with DI H_2O. The aggregation and re-dispersion process was repeated 3 or 4 times to remove the surfactant completely. EDS and XPS were then used to quantify the amount of ZrP residue in the SWCNT aggregates. For TEM observation, the cleansed SWCNTs were

re-dispersed in a mixture of ethanol and hexane with a volume ratio of 1 to 0.9. The reason that this solvent mixture was chosen will be explained in Chapter VI.

5.4 Results and Discussion

5.4.1 Spectroscopy and Microscopy

The dispersion states of SWCNTs before and after SWCNT-ZrP separation were studied using UV-vis-NIR spectroscopy and TEM. As shown in Figure 5.2A, the aqueous solution of pre-treated SWCNTs has limited absorption in the NIR region due to tube bundling (black line) while the SWCNT-ZrP hybrid exhibits much stronger NIR absorption (red line), indicating the presence of a large amount of individually dispersed SWCNTs.[17, 39] No distinct van-Hove transition peaks are observed until SDS is added (blue line). The 1st order van Hove transitions in the NIR region is related to the direct band-gap absorption of individual SWCNTs and is commonly used as an indicator of the dispersion state of SWCNTS.[17, 55] However, the intensity of the van-Hove transitions of different SWCNT species can be affected to a different degree by many factors, such as excessive electrolytes, solution acidity and the type of dispersants chosen.[17, 57-58] Moreover, sharp and strong van Hove peaks do not necessarily preclude the presence of small SWCNT bundles.[17, 57] Therefore, TEM or atomic force microscopy is also required to confirm the dispersion state of SWCNTs.

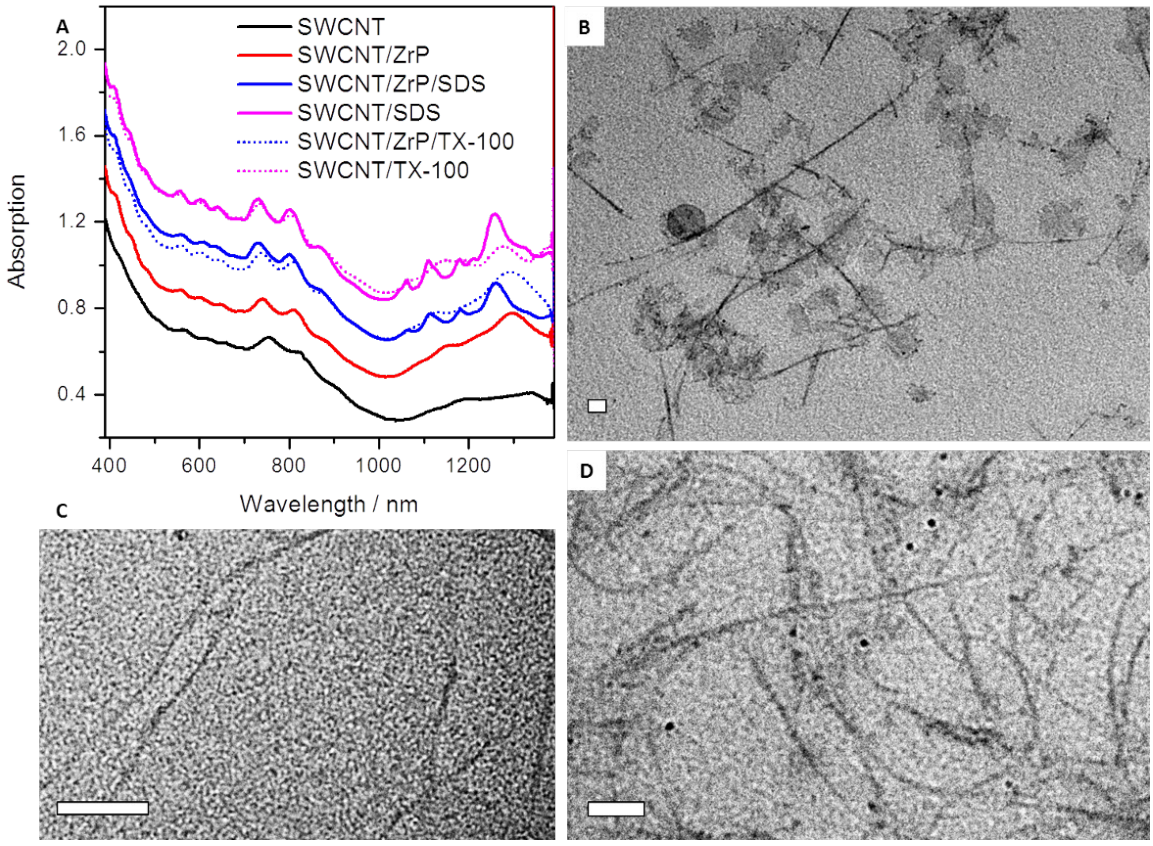

Figure 5.2. (A) UV-vis-NIR spectra of aqueous solutions of pre-treated SWCNTs (black line), SWCNT-ZrP conjugate (red line), SWCNT/ZrP/SDS mixture (blue line) and SWCNTs isolated by SDS (pink line). The dotted blue and pink lines are for SWCNT/ZrP/TX-100 and SWCNTs isolated by TX-100, respectively. (B-D) TEM micrographs of (B) SWCNT-ZrP hybrid, (C) SWCNTs isolated by SDS and (D) SWCNTs further isolated from SDS and re-dispersed in an ethanol-hexane mixture (scale bar is 50 nm).

As shown in Figure 5.2B, all the SWCNTs dispersed by ZrP appear to be individually exfoliated and straightened. After being isolated by SDS, aggregated and

cleaned to remove ion residue, and re-dispersed in a 0.5% SDS solution, the NIR absorption of SWCNTs (pink line) has a similar feature to that of the SWCNT/ZrP/SDS mixture, suggesting that the removal of ZrP does not affect the dispersion state of SWCNTs. However, it is difficult to observe SWCNTs using TEM in the presence of SDS (Figure 5.2C). Therefore, SWCNTs were further isolated from SDS and re-dispersed in a mixture of ethanol and hexane by sonication. TEM of the re-dispersed SWCNTs shows no ZrP or SDS coating; and the SWCNTs remain individually dispersed (Figure 5.2D).

It is noted that the $[H^+]$ needed to achieve optimal separation is quite different for the two surfactants. As shown in Figure 5.3A, the SWCNT-ZrP conjugate contains a large quantity of P and Zr while the pre-treated SWCNTs contain none. When 1% SDS is used to assist the SWCNT-ZrP separation, ZrP begins to aggregate at $[H^+]$ = 0.50 mM and 1.0 mM of HCl can precipitate all ZrP. Figure 5.3A also shows that at complete SWCNT-ZrP separation, neither Na nor S is present in the isolated and purifiied SWCNTs. On the other hand, >1.50 mM of HCl is needed to separate ZrP from SWCNT with 1% TX-100 and full separation happens at $[H^+]$ = 2.00 mM (Figure 5.3B). Figure 5.3C presents the element maps of SWCNT-ZrP conjugate before separation, SWCNTs isolated by SDS at $[H^+]$ = 1.00 mM, and SWCNTs isolated by TX-100 at $[H^+]$ = 2.00 mM. The complete removal of ZrP (green dots) is evident in both cases. Both SDS and TX-100 are able to stabilize about 80% of SWCNTs upon full removal of ZrP.

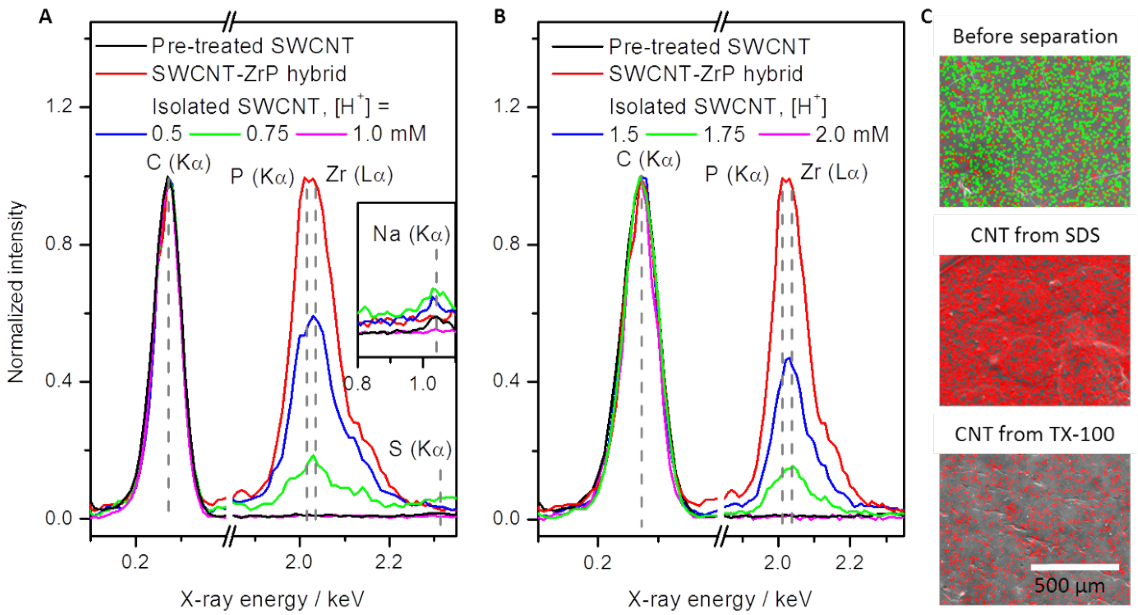

Figure 5.3. (A) EDS spectra of pristine SWCNTs, SWCNT-ZrP hybrid and SWCNTs isolated by 1% SDS at different [H^+]. (B) EDS spectra of pristine SWCNTs, SWCNT-ZrP hybrid and SWCNTs isolated by 1% TX-100 at different [H^+]. (C) Element maps of SWCNT-ZrP conjugate before separation (top), SWCNTs isolated from ZrP by SDS at [H^+] = 1.00 mM and further isolated from SDS (middle), and SWCNTs isolated from ZrP by TX-100 at [H^+] = 2.00 mM and further isolated from TX-100 (bottom). The green dots represent phosphorus, the red dots are carbon and the gray background is aluminum substrate.

Compared with the ionic approach to separate SWCNTs and ZrP described in the previous chapter, the SWCNT yield of the acid-mediated method is lower by about 10% at the optimum separation condition. Figure 5.4 shows the XRD pattern of dry samples

of ZrP exfoliated by TBA, ZrP destabilized by KCl, and ZrP destabilized by HCl. The inset is the diffraction pattern with the diffraction intensity of destabilized ZrP enhanced. The exfoliated ZrP has an interlayer space of about 36 Å. Both ZrP destabilized by KCl and HCl exhibit a nearly amorphous feature. However, the XRD patterns shown in the inset indicate that the nanoplatelets destabilized by HCl might possess a more compact structure. It is possible that more SWCNTs are trapped in the relatively denser ZrP during the separation process, resulting in less SWCNTs retreived by surfactants.

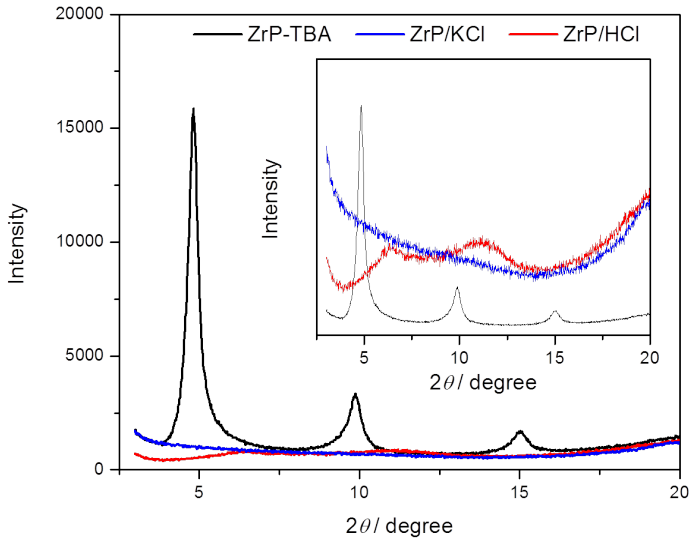

Figure 5.4. XRD patterns of ZrP exfoliated by TAB (black line), ZrP destabilized by KCl (blue line) and ZrP destabilized by HCl (red line).

5.4.2 Dependence on Surfactant Type—The Difference between SDS and TX-100

Titration experiments were further carried out to investigate the difference between the two surfactants. To simplify the scenario, three systems were prepared without SWCNTs: 0.04% of exfoliated ZrP dispersion containing 1% TX-100, 1% SDS, or no surfactant. The mixtures were titrated with 100 mM HCl and the titration curves are plotted in Figure 5.5. Similar curves between ZrP alone and ZrP/TX-100 dispersions indicate that TX-100 does not participate in the acid-base reaction. The equivalence point for these two solutions is around pH = 5 with 0.37 mM HCl added. On the contrary, the addition of SDS alone can reduce the pH value of the ZrP dispersion from 7.5 to 6.4 and the equivalent point appears much earlier with only half of H^+ input (0.18 mM). It is likely that the SDS dissociated when dissolved in water, and the dodecyl sulfate anion ($C_{12}OSO_3^-$) hydrolyzes and generates a hydronium ion, with hydrolysis products composed of a weak base of dodecanol and a strong acid HSO_4^- (p*K*a = 2.0).[65-66] As a result, the pH value is lowered at the beginning of titration and less acid is required to reach the equivalence point. The reverse hydrolysis reaction also leads to a buffer-like feature at the later stage of titration, where the decreasing trend of pH value in the ZrP/SDS dispersion is slower than the ZrP dispersion and the ZrP/TX-100 dispersion, likely due to excess protons absorbed by SDS micelles.

For both SWCNT/ZrP/SDS and SWCNT/ZrP/TX-100 dispersions, the required amounts of HCl for a complete SWCNT-ZrP separation are higher than the equivalence points of their titrated counterparts without SWCNTs. It is possible that the binding between SWCNTs and ZrP hinders the detachment of TBA from the ZrP nanoplatelets

within the time frame of interest. However, the ratio between the optimum [H^+] for SWCNT-ZrP separation and the ratio between the equivalence points between the dispersion containing SDS and the one containing TX-100 are about the same (approximately 0.5). This suggests that the different degree of involvement of surfactants in the acid-base reaction are likely responsible for the different [H^+] requirement for SWCNT-ZrP separation in the two systems.

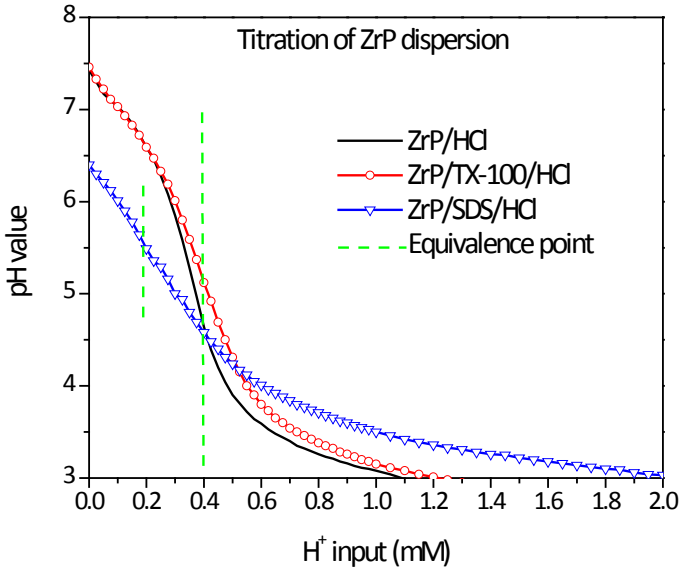

Figure 5.5. Titration curves of 0.04% exfoliated ZrP dispersion without surfactant (black line), with 1% TX-100 (red line), and with 1% SDS (blue line). The green dashed lines indicate the [H^+] equivalence points.

To further understand the effect of hydrolysis of SDS on the SWCNT-ZrP separation, a set of 0.04% ZrP-TBA dispersion with different levels of SDS

concentrations ([SDS]) was prepared. The pH values of the ZrP/SDS mixtures are plotted versus [SDS] in Figure 5.6A, showing an interesting minimum at 0.2%, which is about the critical micelle concentration (CMC) of SDS. The relative hydrolysis rates versus [SDS] were plotted in Figure 5.6B. The hydrolysis rate approaches zero when [SDS] is beyond 1%. SDS with concentrations higher than 3% does not facilitate the acid-induced isolation of SWCNTs. Rather, the isolation process could be retarded. SDS at 1% is most commonly used and generally considered the optimum concentration for HiPco SWCNT dispersion.[57, 67] The current finding also supports such a practice since 1% SDS can reduce the required H^+ amount for SWCNT isolation by half.

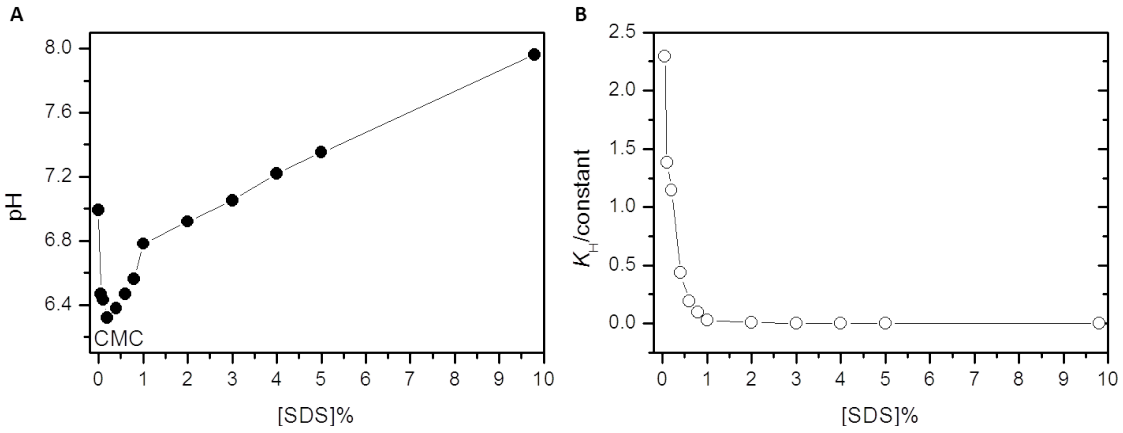

Figure 5.6. Hydrolysis effect of SDS in a 0.04% ZrP-TBA dispersion. (A) pH versus [SDS]. (B) Hydrolysis rate versus [SDS].

An attempt has also been made to use a cationic surfactant, i.e., CTAB, to assist the acid-induced SWCNT isolation. However, CTAB either stabilizes both SWCNT and ZrP at the same time or causes their co-precipitation, depending on the concentrations of SWCNT, ZrP and H^+. Therefore, CTAB cannot be used with acid to separate SWCNT and ZrP.

5.4.3 Isolation of SWCNTs from the Surfactants and Re-dispersion in Various Media

As described above, after separation from ZrP, SWCNTs need to be further isolated from surfactants for an accurate determination of the separation efficiency. This can be achieved by repeated precipitation and dispersion of SWCNTs. The agglomeration of SDS-stabilized SWCNTs can be easily triggered by introducing acetone into the aqueous solution since SDS is insoluble in acetone and SWCNTs have more affinity to acetone than to water. Consequently, SDS and SWCNTs are separated into different phases and are no longer in contact. Afterward, the SDS residue in the re-aggregated SWCNTs can be removed using about 3 washing cycles with a polar solvent such as water or methanol. The absence of SDS residue in the isolated SWCNTs is verified by EDS (Figure 5.3A) and XPS. The purified SWCNTs can be re-dispersed in various solvents to determine a good solvent for individual SWCNTs, as shown in Chapter VI. Moreover, the temporary aggregation state during these procedures does not affect the exfoliation state of SWCNTs if the SWCNTs is are kept in a wet state before re-dispersion in an appropriate solution as shown in Figure 5.3D.

When a conductive strip is drawn using an aqueous ink that contains exfoliated SWCNTs, a nearly perfect 2-D conductive network is formed after water evaporation. This SWCNT network, which contains 12% SDS, exhibits similar electrical conductivity as pristine SWCNTs.[64] This suggests that the presence of a small amount of surfactant would not necessarily be an issue for some device applications. Therefore, the SDS approach to retrieve SWCNTs from the exfoliated SWCNT-ZrP hybrid is highly efficient for obtaining high quality SWCNTs with good dispersion in aqueous solution.

When a non-ionic surfactant is used to assist the SWCNT-ZrP separation, it becomes more complicated to detach SWCNTs from the wrapping surfactants afterwards. SWCNTs can be aggregated by an excess amount of ions or acetone and re-dispersed in DI H_2O. Most TX-100 can be removed from SWCNTs after a few cycles of aggregation and re-dispersion process. Dialysis can expedite the process of removing or replacing the non-ionic surfactants from CNTs.[59] However, for certain types of non-ionic surfactants, such as PVA and PVP, which have been reported to have robust association with HiPco SWCNTs,[40c] it becomes extremely difficult to remove these surfactants thoroughly. A method of preparing nanocomposites based on these water-soluble polymers and SWCNTs directly prepared from the SWCNT-enriched supernatants after SWCNT-ZrP separation will be proposed in Chapter VIII.

5.4.4 A 2-in-1 Step of Functionalization and Stabilization of Individual CNTs into Organic Media

Functionalization of the exfoliated CNTs can also be carried out directly in the SDS- and CNT-enriched supernatant after ZrP is removed, avoiding extra steps of

isolating SWCNTs from SDS. In essence, a functionalizing agent (solution), such as octadecylamine powder or sulfanilamide in acetone, can be added into the CNT-enriched aqueous solution at an elevated temperature (APPENDIX B). The functionalized CNTs become hydrophobic and can be easily re-dispersed in organic solvents and polymer matrices (APPENDIX B). Conductive polypropylene nanocomposites based on multi-walled CNTs (MWCNTs) have been prepared in this manner, with an electrical percolation threshold of CNT concentration among the lowest reported.

5.5 Conclusions

An acid-mediated separation route has been developed to isolate individually dispersed CNTs from the electrostatically tethered ZrP nanoplatelet dispersant for both SWCNTs and MWCNTs. The acid addition causes the detachment of the functional groups on the nanoplatelets, which then causes destabilization and aggregation of ZrP. With incorporation of appropriate surfactants, about 80% exfoliated SWCNTs can be stabilized after the removal of ZrP. The acquired SWCNTs are ZrP-free and remain exfoliated in the solvent of interest. It has been demonstrated that both anionic (SDS) and non-ionic (TX-100) surfactants are effective in stabilizing SWCNTs and MWCNTs and their different roles have been investigated. Examples of applications based on the individually dispersed CNTs using the acid-SDS approach have been demonstrated.

CHAPTER VI

DISPERSION AND STABILIZATION OF PURIFIED NANOPARTICLES USING DIELECTRIC-CONSTANT-MATCHED SOLVENTS

6.1 Introduction

In this chapter, we report a general approach to stabilize and disperse surfactant-free NPs using dielectric-constant-matched solvents. Three different NPs—1-D ZnO QDs, 2-D individual SWCNTs and 3-D ZrP nano-sheets have been selected to demonstrate that individual NPs can be stabilized solely with solvents through the minimization of van der Waals force. The NP stabilization is realized by matching the dielectric constant (or permittivity, ε) of the NPs and the media. Highly stable NP dispersions haven been prepared by using proper binary solvent mixture; afterward, individual NPs can be transferred and stabilized in appropriate single-component solvents. This generalized approach of dispersing and stabilizing NPs opens a new avenue for fundamental understanding of the thermodynamics of NP colloids and can be useful in manipulating the dispersion state of NPs in solvents and polymer matrices.

6.2 Working Principle

As introduced in Chapter I, Hamaker's summation principle can be used to estimate the vdW potential between two macroscopic (compared to atoms and molecules) blocks.[2-3] The resulting vdW interaction is usually given in terms of the conventional Hamaker constant, which is a measurable constant for bulk material but

can also be calculated using Dzyaloshinskii-Lifshitz-Pitaevskii (DLP) theory based on bulk dielectric properties of the block materials.[2]

The resolved interparticle vdW potential is dependent on the geometries of the blocks, that, for two sphere-like particles,

$$\Phi_{\mathrm{vdw}} = \frac{-A}{6d}\frac{\mathrm{r}_1 r_2}{r_1 + r_2} \tag{6.1}$$

where A is the Hamaker constant, d is the interparticle distance, and r_1 and r_2 are the radius of the two particles respectively.[3]

For two rod-like particles,

$$\Phi_{\mathrm{vdw}} = \frac{AL}{12\sqrt{2}d^{3/2}}\left(\frac{\mathrm{r}_1 r_2}{r_1 + r_2}\right)^{1/2} \tag{6.2a}$$

when particles are parallel to each other and l is the length of the rod-like particles,

and $$\Phi_{\mathrm{vdw}} = -A\sqrt{r_1 r_2}/6d \tag{6.2b}$$

when particles are crossed to each other.[3]

For two plates of equal thickness,

$$\Phi_{\mathrm{vdw}} = -\frac{A}{12\pi}\left(\frac{1}{d^2} + \frac{1}{(d+2t)^2} - \frac{2}{(d+t)^2}\right) \tag{6.3}$$

where d is the interparticle distance and t is the thickness of the plate-like particles.[2]

Therefore, for all three types of the NPs, Φ_{vdw} equals zero when A equals zero, which means there is no net attractive interaction between the NPs.

DLP theory indicates that,

$$A_{213} = \frac{3}{8\pi^2}h\int_0^{\infty}\left[\frac{\varepsilon_2(i\xi) - \varepsilon_1(i\xi)}{\varepsilon_2(i\xi) + \varepsilon_1(i\xi)}\right]\left[\frac{\varepsilon_3(i\xi) - \varepsilon_1(i\xi)}{\varepsilon_3(i\xi) + \varepsilon_1(i\xi)}\right]d\xi \tag{6.4}$$

where ε_2 and ε_3 are the dielectric constants of the two blocks, respectively, ε_1 is the dielectric constant of the media spacing the blocks and $i\xi$ is the imaginary frequency axis.[2]

In general, the DLP theory is complicated to apply except for the simplest case, where the two blocks are identical ($\varepsilon_2 = \varepsilon_3$) and the block material and the media have the same dielectric constants ($\varepsilon_1 = \varepsilon_2 = \varepsilon_3$) at all frequencies. In this case, the A_{213} equal zero, corresponding to no net vdW interaction.[2] Thus, the effect of vdW attraction can be compensated by an appropriate media.

Although it is not likely that the dielectric constants of the particles and the media can be exactly matched at all frequencies,[2] a few practices with NPs have aroused our attention in applying the principle in dispersion of purified, surfactant-free and individually dispersed NPs. In our precious work, we noticed that the addition of hexane slows the aggregation of purified ZnO QDs that is originally dispersed in methanol.[29] ZnO QDs in chlorobenzene/methanol mixture has also been found to be well-dispersed when blended and spin coated with a polymer,[68] compared with the composite of polymer and ligand-capped ZnO QDs.[69] In this chapter, we demonstrate that purified ZnO QDs can be individually dispersed in a dielectric-constant-matched solvent with long-term stability. Two other NPs with different geometries—SWCNTs and ZrP nanoplatelets have also been used to show that the approach is applicable with various types of NPs.

6.3 Experimental

6.3.1 Purification and Dispersion of ZnO QDs

The ZnO-methanol sol was obtained using the method described in Chapter III.[44] The prepared ZnO sol contains a large quantity of K^+ and acetates, and the electrostatic repulsion between the ZnO QDs keeps them from forming aggregation. In order to purify the ZnO QDs, hexane and isopropanol was added with a volumetric ratio of QD-methanol dispersion: hexane: isopropanol = 1: 5: 1.[29] A considerable fraction of ZnO QDs precipitated after resting the dispersion overnight at 4 °C and can be re-dispersed in methanol. The precipitation and re-dispersion was repeated 4 times to remove excess ions.[29] In the last cycle, the precipitated ZnO was re-dispersed in a series of 4 ml mixture of methanol and dichloromethane with a ZnO concentration ([ZnO]) of 0.4 M and volume fraction of methanol (φ(methanol)) that equals 1.0, 0.70, 0.50, 0.30, 0.20, 0.10 and 0. The re-dispersed colloidal ZnO is denoted as ZnO-M0, ZnO-M70, ZnO-M50, …etc. The samples were observed at room temperature to determine their stability. It is found that the ZnO-M50 is the most transparent when prepared and has the best stability over time compared with other systems.

To transfer the well-dispersed ZnO QDs into a single-component solvent, 4 ml ZnO-M50 was added drop wisely under stirring to 4 ml of 1-butanol (ε = 17.54), 1-pentanol (ε = 14.96), 1-hexanol (ε = 13.06), 1-heptanol (ε = 11.41) and 1-octanol (ε = 10.01) at 80-90 ^{o}C. The temperature was chosen because it is above the boiling points of methanol and dichloromethane and below the boiling points of the other alkyl alcohols. The value of ε is from the Landolt-Borstein Database hereafter.

6.3.2 Purification and Dispersion of SWCNTs

Individual SWCNTs were isolated from ZrP nanoplatelets dispersant by SDS using the acid-mediated isolation approach described in Chapter V. The SWCNTs were further isolated from SDS solution by acetone addition which causes the aggregation of SWCNTs. The re-aggregated SWCNTs were cleansed with methanol for 3 times and re-dispersed in water (ε = 80.4), methanol (ε = 32.6), ethanol (ε = 24.3), n-hexane (ε = 1.9), ethanol-hexane mixture with a 1:0.9 volume ratio, 1-propanol, 1-butanol, 2-butanl (ε = 16.58), 3-methyl-1-butanol (ε = 15.8), 1-pentanol and 1-hexanol by sonication.

To prepare suspension of SWCNT bundles, pre-treated SWCNTs were dispersed in 1% SDS solution by sonication and isolated from SDS by adding acetone to precipitate the SWCNTs. The isolated SWCNT bundles were then cleaned and re-dispersed in 1-propanol, 1-butanol, 2-butanl, 3-methyl-1butanol, 1-pentanol and 1-hexanol by sonication.

6.3.3 Preparation and Dispersion of Purified ZrP Nanoplatelets and K^+ Functionalized ZrP Nanoplatelets (ZrP-K)

After the synthesized ZrP was exfoliated by TBA^+OH^- with a molar ratio of 1 to 1, the nanoplatelets were agglomerated by adding acid. The coagulated nanoplatelets were washed 3 or 4 times with DI H_2O to remove acid and TBA residue. The purified ZrP was dispersed in a series of mixtures of ethanol and DI H_2O with a ZrP concentration of 0.05% and volume fraction of ethanol (φ(ethanol) equals to 0, 0.25, 0.33, 0.5, 0.67, 0.75, 0.80, 0.83, 0.86, 0.89 and 1.0.

To prepare ZrP-K, the purified ZrP nanoplatelets were immersed in 100 mM KOH aqueous solution for 30 min and washed with DI H_2O for 3 or 4 times to remove additional KOH. The modified nanoplatelets containing the K^+ in the ZrP structure were then re-dispersed into DI H_2O *via* sonication.

6.4 Results and Discussion

6.4.1 Stability of ZnO QDs

i. ZnO QDs dispersed in binary mixture of methanol and dichloromethane

The photographical images of dispersions of purified ZnO QDs in the binary mixture of methanol and dichloromethane are shown in Figure 6.1. In each image, from left to right, φ(methanol) = 1, 0.70, 0.50, 0.30, 0.20, 0.10 and 0. As prepared, all ZnO dispersions are transparent in appearance except ZnO-M0 and ZnO-M100 (Figure 6.1A), which quickly turned turbid and began to precipitate. UV-vis spectroscopy was utilized to quantitatively differentiate the transparency among the systems. As shown in the transmission spectra (Figure 6.2A), both ZnO-M0 and ZnO-M100 exhibit significant light scattering due to the aggregation of ZnO QDs. ZnO-M10 and ZnO-M20 also show slight light scattering and a small degree of opacity. While the transmission spectra of ZnO-M30, ZnO-M50 and ZnO-M60 are similar, ZnO-M50 appears to be most transparent. The results suggest that the QDs in ZnO-M50 are most stable and tend to remain dispersed for an extended period of time. Indeed, QDs in ZnO-M0 and ZnO-M100 began to precipitate after 1 day. Interestingly, the QD sediment in ZnO-M0 is less than that in ZnO-M100. The ZnO-M100 contains a loose white layer of QD aggregates,

while the precipitates in ZnO-M0 (outlined by the red circles) can barely be seen. It is likely that most small QDs in ZnO-M0 remained dispersed after 1 day while most QDs in ZnO-M100 formed cluster and precipitated. ZnO-M10 turned cloudy from transparent after 1 day (Figure 6.1B). QDs in ZnO-M70 also began to precipitate after 1 week (Figure 6.1C). Only ZnO-M50 remains transparent after 1 month (Figure 6.1D), suggesting the best stability of the QDs in the solvent mixture. The results are in agreement to the UV-vis spectra taken when all samples were freshly prepared. Therefore, UV-vis spectra can be used to determine the stability of the QD dispersion in early stage of aggregation.

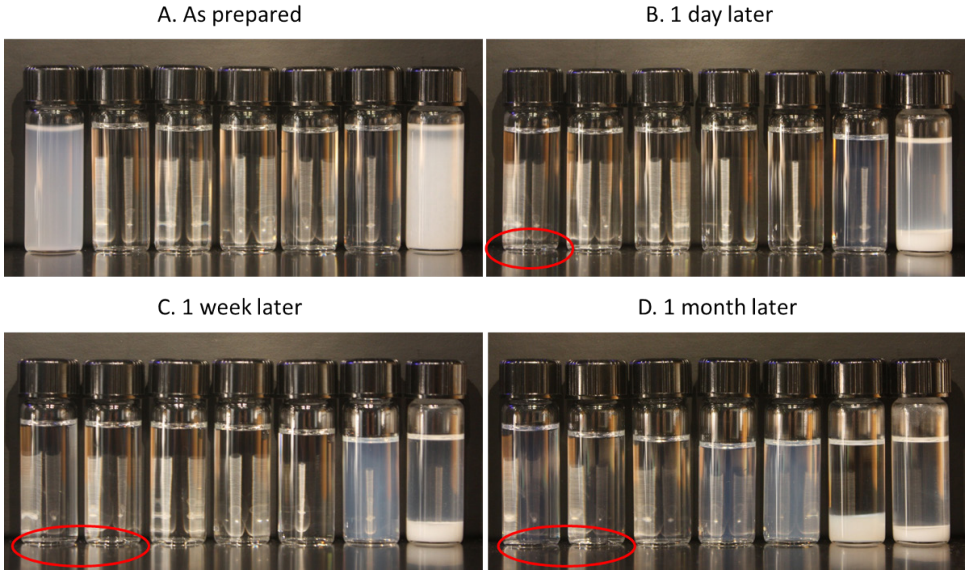

Figure 6.1. Purified ZnO in binary mixture. The dispersions are (A) as prepared, (B) after 1 day, (C) after 1 week and (D) after 1 month at room temperature. [ZnO] = 0.4 M. φ(methanol) = 1.0, 0.70, 0.50, 0.30, 0.20, 0.10 and 0 from left to right. The red circles indicate precipitates than can be seen by bare eyes but are not visible on the images.

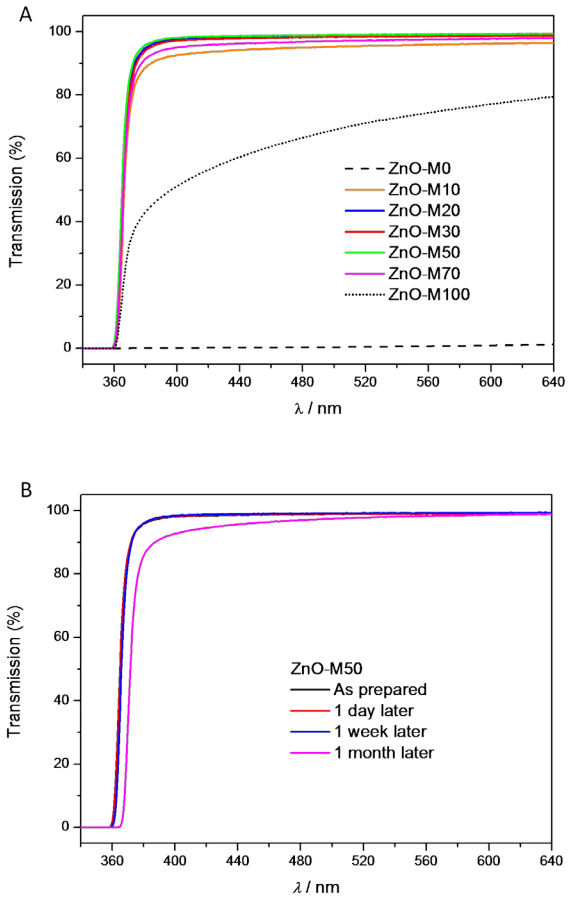

Figure 6.2. UV-vis spectra of (A) ZnO-M0, ZnO-M10, ZnO-M20, ZnO-M30, ZnO-M50, ZnO-M70 and ZnO-M100 at the time of preparation, and (B) ZnO-M50 at different time.

The UV-vis transmission spectra of ZnO-M50 at different stages are shown in Figure 6.2B. The transparency of the sample remained for 1 week. However, their hazy appearance can be detected after 1 month. The transparency can be maintained much longer for diluted samples or samples stored at lower temperature (4 ^{o}C). Although the

transparency is reduced with time, the stability of the sample is still outstanding. As mentioned above, the ZnO QDs were prepared in methanol solution containing a large quantity of K^+ and acetate ions. The QDs are metastable owing to the electrical double layer repulsion. On the other hand, the ZnO-methanol sol turns turbid within 24 hours at room temperature. Even at 4 ^oC, the transparency of the ZnO sol cannot be maintained longer than 3 days. Therefore, the observed long-term stability of purified ZnO QDs in ZnO-M50 is quite significant.

ii. ZnO QDs dispersed in single-component solvents.

Figure 6.3 shows the photographical images of ZnO QDs transferred from ZnO-M50 to various single-component solvents at 80-90 ^oC. From left to right, the medium is 1-butanol, 1-pentanol, 1-hexanol, 1-heptanol and 1-octanol, with decreasing ε. None of 1-butanol, 1-pentanol and 1-octanol can provide long term stability of QDs. The QDs in 1-butanol and 1-pentanol turned turbid during the sample preparation (Figure 6.3A) and the QDs in 1-octanol turned cloudy in 2 hours (Figure 6.3B). QD/1-hexanol stayed transparent until 4 days later (Figure 6.3C); the transparency of QD/1-heptanol maintained after 8 days (Figure 6.3D).

The UV-vis transmission spectra of freshly prepared samples also show that QD/1-heptanol is the most transparent (Figure 6.4A). The results suggest that 1-heptanol is the best solvent for purified ZnO QDs. The transmission spectra of QDs dispersed in 1-heptanol at different time is shown in Figure 6.4B. Significant light scattering can be observed 16 days after preparation. The stability of QD-1-heptanol dispersion is not as

good as ZnO-M50, suggesting that ZnO may have aggregated or grown during the heating process of transferring the QDs.

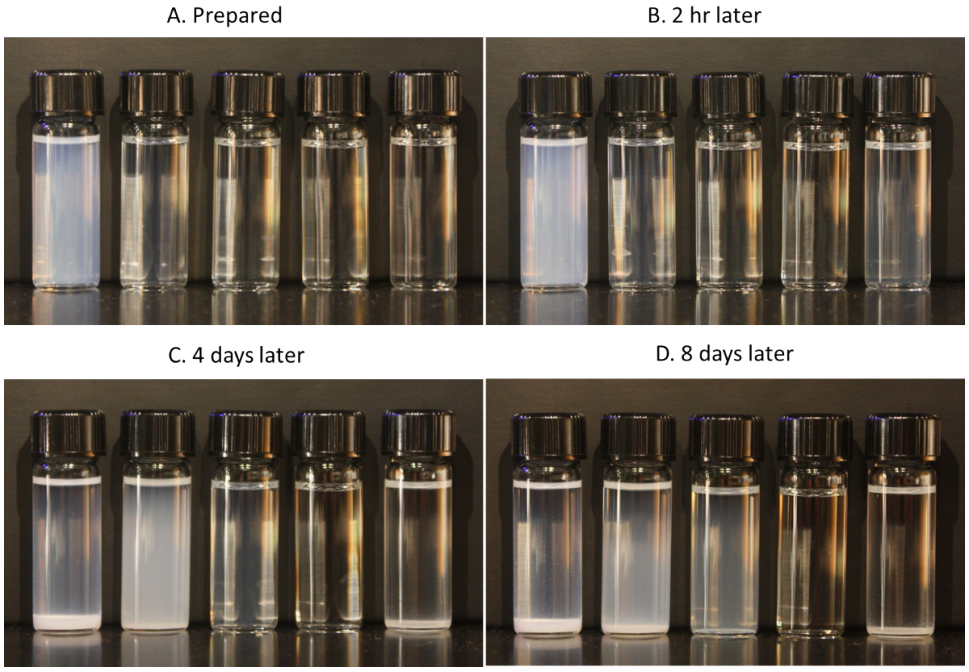

Figure 6.3. ZnO QDs transferred to various single-component solvents (A) at the time of preparation, (B) 2 hours later, (C) 4 days later and (D) 8 days later. [ZnO] = 0.4 M. The media is 1-butanol, 1-pentanol, 1-hexanl, 1-heptanol and 1-octanol from left to right.

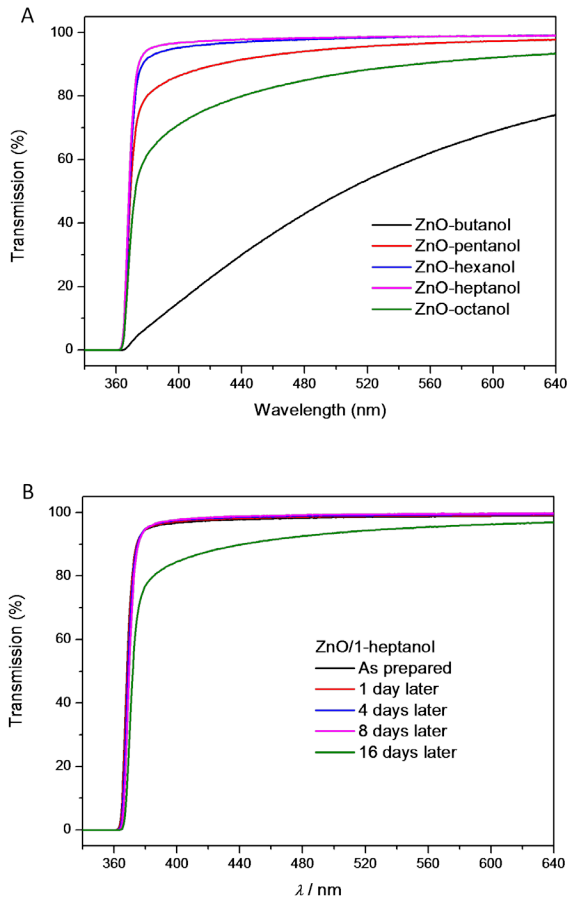

Figure 6.4. UV-vis transmission spectra of (A) ZnO QDs transferred into 1-butanol, 1-pentanol, 1-hexanl, 1-heptanol and 1-octanol, and (B) ZnO/1-heptanol dispersion at different time.

It is noted that the ε values of the good binary solvent and the good single-component solvent for purified QDs are quite different. According to ref. [70], methanol-dichoromethane has a ε of 24.81 when φ(menthol) = 0.50,[70] while 1-heptanol

has a ε of 11.41. According to literature, the ε value is between 9.9 to 11 for bulk ZnO material and is between 10.8 to 11 for polycrystalline ZnO film.[71] The disagreement in the ε of the two good solvents for ZnO NPs could be due to the size-dependent dielectric properties of the ZnO NPs, that, the larger the particle is, the less polar the particle appears to be.[72] A similar trend has been observed for individual SWCNTs and SWCNT bundles as will be discussed later. TEM micrographs of the ZnO QDs in ZnO-M50 and 1-heptanol are shown in Figure 6.5A and Figure 6.5B, respectively. Indeed, the particle size of ZnO QDs in 1-heptanol appears larger than those in ZnO-M50.

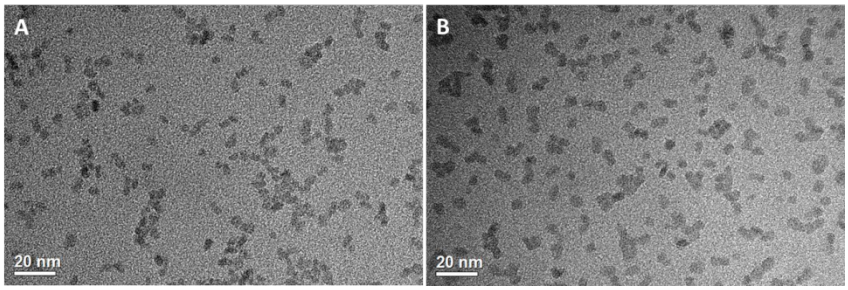

Figure 6.5. TEM micrographs of ZnO QDs in (A) ZnO-M50 and (B) 1-heptanol at the time of preparation. The latter has a larger average particle size.

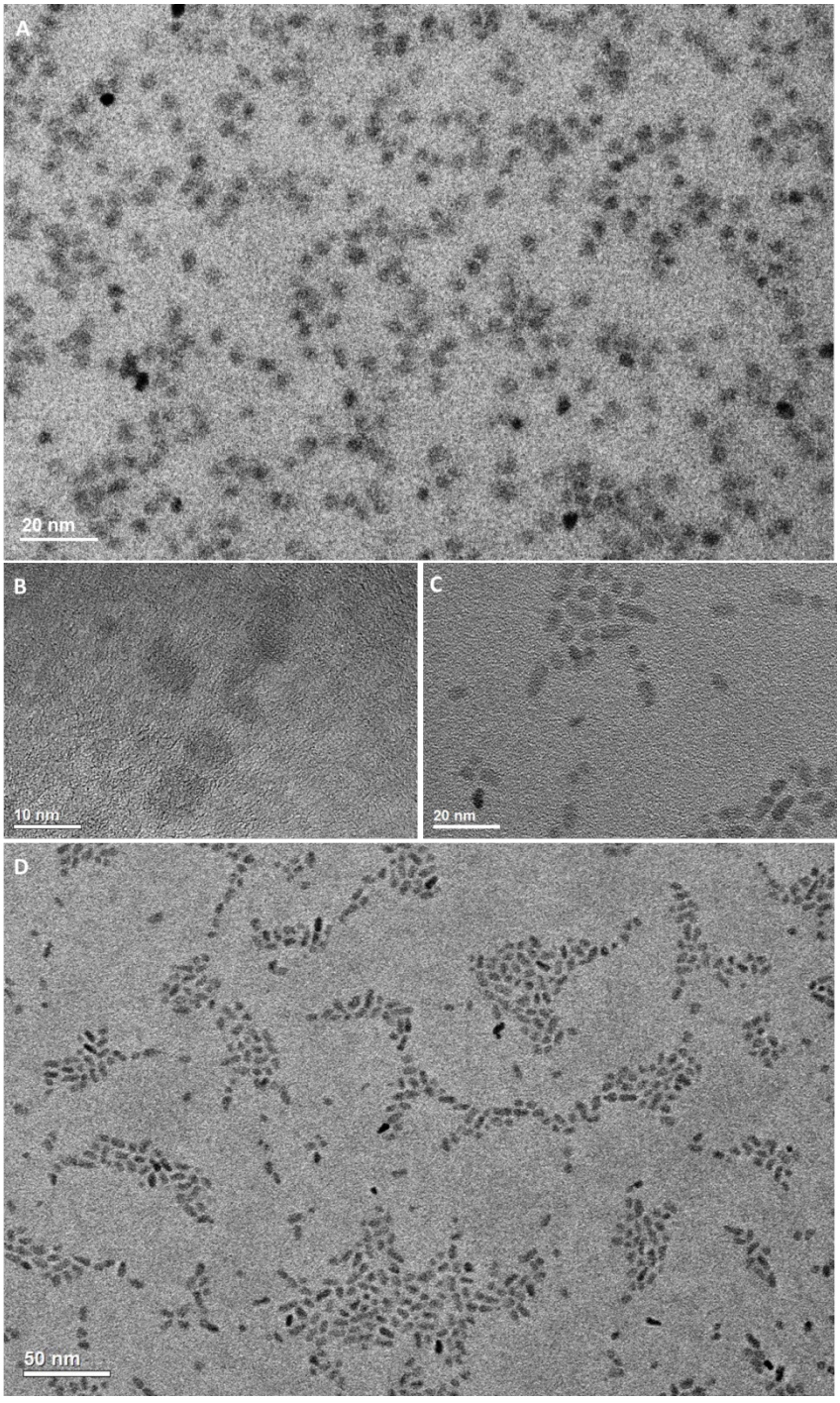

Figure 6.6. (A, B) ZnO QDs in ZnO-M50 at the time of preparation and (C, D) fused ZnO QD dimers in ZnO-M50 after 1 month.

Another interesting phenomenon is that for ZnO-M50, almost all ZnO were individually dispersed when prepared (Figure 6.6A). However, in some regions, the QDs tend to align along the same lattice direction (Figure 6.6B). After one month, the ZnO-M50 dispersion became slightly hazy. At this point, almost all ZnO QDs fused into short rods with an average length of about 2 QDs (Figure 6.6C). To our knowledge, the ZnO QD dimers are the shortest among the nanorods reported and appear to be uniformly dispersed (Figure 6.6D). The above finding suggests that while choosing a solvent with minimized dielectric constant differences, the intermediate solvent is capable of compensating the interparticle vdW attraction between ZnO QDs, at least to certain extent; however, the strong interatomic bonding strength (≤ 250 KJ/mol) could still render adjacent ZnO to merge along the same lattice orientation.[73]

6.4.2 Stability of SWCNTs

Figure 6.7 shows the photographical images of individual SWCNTs dispersed in methanol, ethanol, ethanol-hexane mixture and hexane. SWCNTs in hexane precipitate immediately after preparation. While in methanol, SWCNTs precipitate within 24 hours (not shown). These suggest that water, methanol and n-hexane are not good solvents for SWCNTs. The visual appearances of SWCNTs in ethanol and ethanol-hexane mixture appear similar. Hence, TEM has been performed to examine their possible morphological difference.

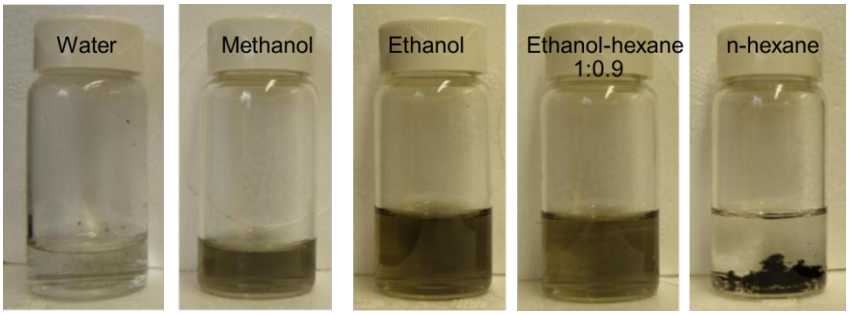

Figure 6.7. Individual SWCNTs isolated from ZrP by SDS and cleaned and re-dispersed into water, methanol, ethanol, ethanol-hexane mixture with a 1 to 0.9 volume ratio, and n-hexane.

As shown in Figure 6.8, the SWCNTs dispersed in ethanol exist primarily as individual nanotubes but small bundles of SWCNTs can also be observed. On the contrary, the SWCNTs dispersed in ethanol-hexane mixture are all present as individual tubes. Therefore, the ethanol-hexane mixture with a 1 to 0.9 volume ratio is likely a good solvent for dispersing surfactant-free individual SWCNTs.

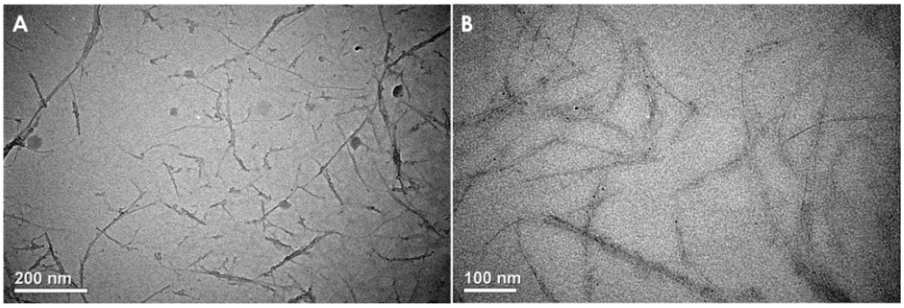

Figure 6.8. TEM micrographs of SWCNTs dispersed in ethanol (left) and ethanol-hexane mixture (right).

Individual SWCNTs can also be transferred into a single-component solvent and can be stabilized in 1-propanol, 1-butanol and 2-butanol, but are not stable in 3-methyl-1-butanol, 1-pentanl, nor in 1-hexanol. The difference is not obvious when the samples are freshly prepared (Figure 6.9 A (up)), but can be easily differentiated 24 hours later (Figure 6.9A (bottom)). The optimum condition of preparing samples for TEM observation of the individual SWCNTs in a single-component solvent has not yet been determined. The currently prepared samples show presence of short and branched bundles (Figure 6.9C), which suggests that the SWCNTs should have been exfoliated and re-assembled as short bundles. Suspensions of SWCNT bundles have also been prepared for comparison purposes. As shown in Figure 6.9D, the SWCNT bundles have an average diameter of about 4 nm. The SWCNT bundles begin to precipitate immediately after sonication in most solvents (Figure 6.9B) except when dispersed in 2-butanol, which agglomerates within 24 hours. Although 2-butanol cannot stabilize the SWCNT bundles for long, it is the best solvent for SWCNT bundles among the solvents chosen. Similar to that for ZnO QDs, a good solvent for individual SWCNTs is more polar than that for SWCNT bundles, which could also be because of their size differences.

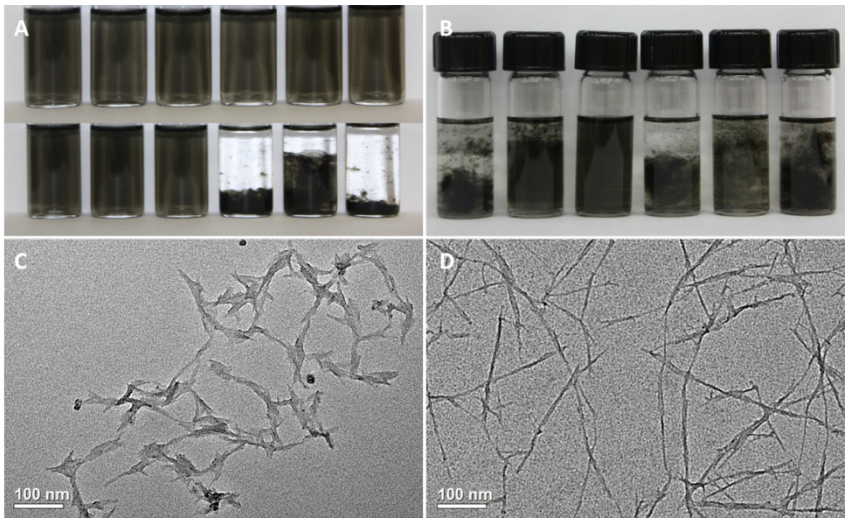

Figure 6.9. (A, B) Photographical images of (A) dispersions of individual SWCNTs at the time of preparation (up) and after 24 hours (bottom), and (B) dispersions of SWCNT bundles at the time of preparation. The solvents from left to right are 1-propanol, 1-butanol, 2-butanol, 3-methyl-1-butanol, 1-pentanol and 1-hexanol. (C, D) TEM micrographs of (C) pre-exfoliated SWCNTs in 1-propanol which form into short and branched bundles and (D) SWCNTs bundles in 2-butanol.

6.4.3 Stability of Purified ZrP Nanoplatelets and ZrP-K

i. Elemental analysis of ZrP nanoplatelet and its derivatives

XPS was used to quantify the chemical composition of the functionalized ZrP nanoplatelets and their derivatives. Table 6.1 lists the atomic ratio of Zr, P, K (if any), O, and C elements of nanoplatelets treated differently and normalized by the amount of Zr element. The superscript "e" denotes the experimental value and the superscript "t" denotes the theoretical value of the chemical structures of $Zr(PO_4)_2K_2$ (ZrP-K),

$Zr(HPO_4)(PO_4)$-$C_{16}H36$ (ZrP-TBA conjugated at a molar ratio of 1:1), and $Zr(HPO_4)_2 \cdot H_2O$ (i.e., purified ZrP) nanoplatelets. The large C content in ZrP-TBA obviously comes from the TBA molecule. After using acid to neutralize TBA, the C content is significantly reduced in the purified ZrP nanoplatelets, indicating the detachment of TBA molecules from the nanoplatelet surfaces. A comparable amount of K to that of P and Zr in ZrP-K nanoplatelet verifies the presence of K^+ on the nanoplatelet structure. The chemical structure of the product is likely to be $Zr(PO_4)_2K_2$ after the HPO_4^{2-} reaction with KOH.

Table 6.1 Chemical composition of various modified ZrP nanoplatelets.

Atomic ratio	P^e/P^t	Zr	K^e	O^e/O^t	C^e/C^t
ZrP-K	1.5/2	1	1.6	7.4/9	3.4/0
ZrP-TBA	2.0/2	1	NA	8.7/9	13/12.8
ZrP	1.9/2	1	NA	8.4/9	5.6/0

ii. Solvent-stabilization of ZrP derivatives

As shown in Figure 5.1A, pristine ZrP nanoplatelets, without TBA-assisted exfoliation, cannot form a stable dispersion. However, with the same chemical composition, the purified ZrP prepared by exfoliation with TBA and TBA removal by acid has been found to be stable in a mixture of ethanol and DI H_2O with φ(ethanol) = 0.67. The dispersion has a similar appearance compared with other dispersion of different solvent mixtures when freshly prepared (Figure 6.10A), but is the only one without any precipitate after 10 months (Figure 6.10B). The results indicate that

exfoliated nanoplatelets do not restack into a highly ordered layered structure even after the detachment of TBA molecules. On the contrary, the ligand-free nanoplatelets aggregate forms a loosely packed structure in its wet state. This allows the re-dispersion of the purified nanoplatelets by matching its dielectric properties with that of the solvent. The purified nanoplatelets should be able to form a stable solution in a single-component solvent with ε of about 43, and can also be modified to become ZrP-K nanoplatelets and remain stable in water, without any noticeable change after 10 months (Figure 6.10C).

Figure 6.10. Photographical images. (A) As prepared dispersion of purified ZrP in binary mixture of ethanol and DI H_2O with φ(ethanol) = 0, 0.25, 0.33, 0.5, 0.67, 0.75, 0.80, 0.83, 0.86, 0.89 and 1.0 from left to right. (B) 16 months after preparation, purified ZrP in binary mixture of ethanol and DI H_2O with φ(ethanol) = 0.33, 0.5, 0.67, 0.75 and 0.80 from left to right. (C) ZrP-K nanoplatelets in DI H_2O.

6.4.4 The Dispersion Mechanism

In this work, several solvents with similar chemical structure were used when transferring the NPs into a single-component solvent. This is to exclude the possibility that the NPs are stabilized through steric repulsion of the conjugated solvent molecules. In that case, molecules with longer chains should be more capable of stabilizing the NPs. According to Equation (6.4), the Hamaker constant A_{213} can never be negative for two identical particles, which means vdW attraction always exists unless the media and the particles have the same ε. Therefore, when ε of the media is larger or smaller than that of the particles, vdW force is likely to cause the aggregation of the particles. A similar trend has been observed for all 3 types of NPs; as the ε of the media increases, the NP dispersions will change from unstable to stable, and to unstable again. These results suggest that purified NPs here are stabilized through the minimization of the vdW force.

6.5 Conclusions

Purified ligand-free NPs have been stabilized in dielectric-constant-matched solvents. Binary mixtures of a polar and a non-polar solvent with significantly different ε are first used to determine the appropriate ε range of a possible good solvent for NPs. NPs are then transferred into several single-component solvents. ZnO QDs are found stable in 1-heptanol and SWCNTs in 2-butanol. ZrP nanoplatelets can also be exfoliated, purified and modified to become stable in water without the use of surfactants. Long-term stability has been observed for all three kinds of NPs dispersed in appropriate solvents. It should be noted that ZnO QDs tend to fuse along the same lattice orientation

to form dimers. Current results also suggest that smaller NPs tend to exhibit high ε than larger NPs.

CHAPTER VII

PHASE BEHAVIOR OF SURFACTANT-FREE ZNO QDS*

7.1 Introduction

In this chapter, the phase behavior of purified ZnO QDs is examined. By carefully manipulating the solvent composition and the ionic strength, the phase transition of colloidal ZnO QDs can be successfully tuned from a stable dispersion, to a gel-like fluid, to a 3-D ordered, or to an amorphous solid. The transition is similar to that established for micro-spheres and is observed with NPs for the first time. XRD, SAXS, SEM and TEM, PL and UV-vis spectroscopy were utilized to characterize the ZnO QDs and their assembled structure. It is found that the interparticle repulsion decreases as the media ionic strength decreases. Colloidal crystals formed at a critical ion concentration remain transparent and maintain a centimeter-sized close-packed structure upon solvent removal, suggesting that it is possible to promote colloidal crystallization of the NPs into large domains by simply tuning the particle–particle interactions. The transparent large-scale crystalline solids comprised of QDs may be suitable for a variety of optical, electrical, and piezotronic applications. Moreover, by using the surfactant-free ZnO QDs as a model system, it becomes possible to unambiguously examine the fundamental phase behavior of NPs through the variation of NP electrostatics.

7.2 Theory

For monodisperse colloidal spheres, close-packed periodic structures are expected to form spontaneously under certain circumstances.[74] For example, the formation of colloidal crystals based on the hard sphere or nearly hard-sphere interactions is simply driven by configurational entropy, that is, when the interparticle force is negligible.[12b, 75] Other than these few extremely simplified systems, the phase behavior of colloidal particles is strongly dependent on the range and magnitude of the particle–particle forces. For many micron-sized spherical particle systems, a criterion has been established that states: within a reasonable period of interest, colloidal particles remain dispersed if the magnitude of the total interparticle attraction at minimum separation (Φ_{min}) is much smaller than that of the thermal energy (kT), but tend to partition from the media and form a condensed phase once Φ_{min} exceeds kT. The particle morphology of the condensed phase can range from a disordered fluid (Φ_{min} is comparable to kT), to ordered solids (Φ_{min} is slightly greater than kT), and to a random flocculation (Φ_{min} is greater than kT) as the interparticle attraction increases (Figure 7.1).[76]

On the other hand, a great deal of uncertainty usually exists in predicting the phase behavior of NPs due not only to their extremely small sizes and the complex force fields among the adjacent NPs, but also to their structural imperfection and the presence of comparable size-scale impurities. The effect of thermal energy imposed on particle kinetics, increases dramatically as the particle sizes reduce down to the nanometer level, rendering it a necessity to utilize surfactants to mediate the interparticle interaction and

colloidal crystallization. Unfortunately, the introduction of surfactants gives rise to additional variables, such as the brush thickness of surfactants,[77] which tends to greatly complicate physical modeling and interpretation of the phase behavior of NPs. In the following section, we will demonstrate that the phase transition of the surfactant-free ZnO QDs, tuned by the media ionic strength, is similar to that of microspheres.

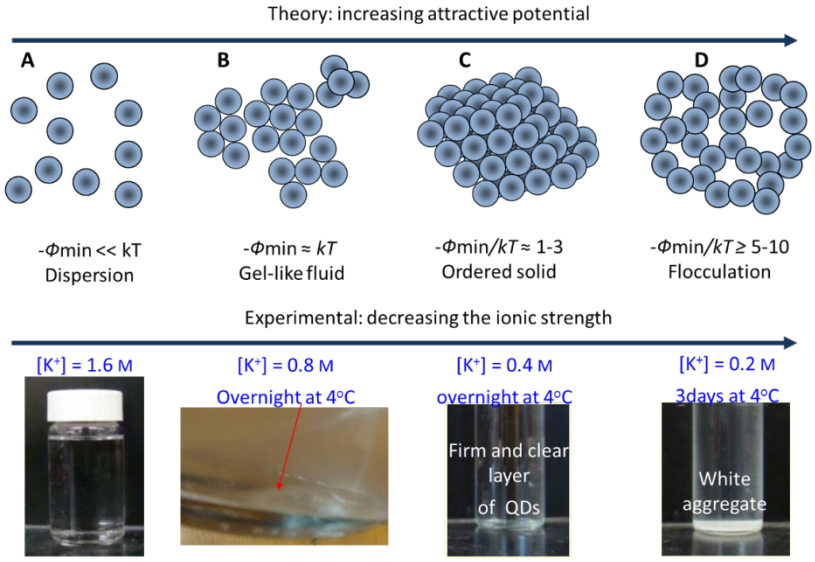

Figure 7.1. Phase behavior of ZnO QD colloids at different ionic strengths. As the media ionic strength decreases, the interparticle attraction increases.

7.3 Experimental

The ZnO-methanol sol was prepared as described in Chapter III. The initial concentration of K^+ ($[K^+]$) in the prepared ZnO was 0.8 M and was adjusted by adding methanol or potassium acetate. Hexane and isopropanol were then added with a

volumetric ratio of QD–methanol dispersion: hexane: isopropanol=1: 5: 1. Usually a considerable fraction of ZnO QDs precipitated after resting the dispersion overnight at 4 ^{o}C. The morphologies of the precipitated ZnO QD ensembles varied with different ion concentrations in the solution. Once a transparent solid layer of ZnO QDs formed at [K^+] = 0.4 M, the supernatant was decanted and the QD layer was left to dry at ambient conditions for SAXS, XRD, TEM and SEM characterization, or secured with a silane-treated cover glass for UV-Vis spectroscopy analysis.

ZnO QD aggregates were prepared by re-dispersing the gel-like QD-rich layer formed at [K^+] = 0.8 M in methanol and then drying at ambient condition. It should be noted that over 95% of the K ions were removed from the ZnO QD ensembles from the above steps.[29]

To prepare samples for TEM characterization, both ZnO QD colloidal crystals and QD aggregates were ground into a fine powder form and dispersed in methanol through sonication. Then, a droplet of the suspension was placed onto a 400-mesh carbon-coated copper grid.

7.4 Results and Discussion

7.4.1 Interparticle Potential and Colloidal Crystallization of ZnO QDs

The XRD pattern of the synthesized ZnO QDs is shown in Figure 7.2. The particle size calculated from the Debye-Scherrer formula $d = 0.89\lambda/(b\cos\theta)$ (d stands for the average diameter of the particles; λ, the X-ray wavelength, 1.5418 Å; b, full width at half maximum, FWHM, of the diffraction peak; and θ, the diffraction angle) is around

5.3 nm. The result is in agreement to the size of individual ZnO QDs observed under TEM (the inset).

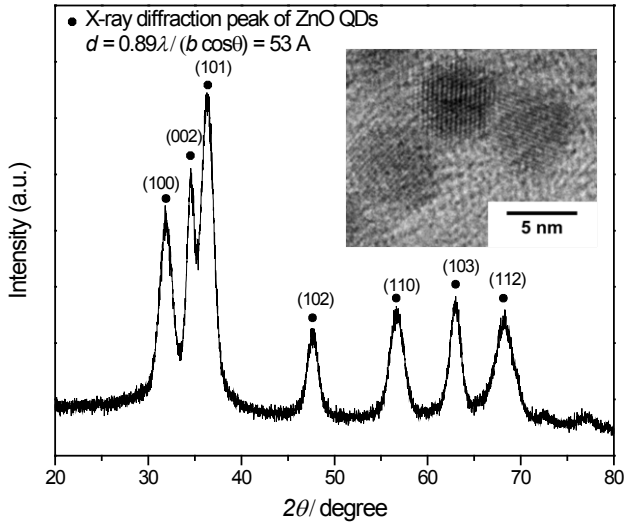

Figure 7.2. XRD powder diffraction of Wurtizite ZnO QDs. The calculated particle size is around 5.3 nm. The inset is a TEM micrograph of individual ZnO QDs in solution.

PL spectroscopy was used to investigate the relationship between the surface state and the interparticle potential. When excited with a 350 nm laser, the ZnO sol exhibits a weak band-edge excitonic emission at 372 nm and a strong donor–acceptor pair luminescence at about 542 nm (Figure 7.3, green line).[78] The UV excitonic emission is significantly blue-shifted compared with bulk ZnO due to the increase in the energy level of the first excited state for quantum-size ZnO.[79] Extensive investigation has shown that the green luminescence of ZnO QDs is originated from the electron

transition from the conduction band edge to a trap level, and the singly ionized oxygen vacancies on the QD surface have been assumed to be the recombination centers.[80] Consequently, dry ZnO QDs show a strong near-band-edge excitonic emission at 382 nm, similar to a commercially available bulk material,[79, 81] but no green luminescence because the surface ionization is completely suppressed (Fiugre 7.3, black line). The surface ionization of ZnO QDs in a highly polar solvent such as methanol also leads to an excess surface charge and an electrostatic interparticle repulsion which keeps QDs individually dispersed until the interparticle repulsion is overcome by vdW attraction. Therefore, the synthesized ZnO sol is transparent and stable at room temperature for a few hours without aggregation. The transparency of the ZnO sol can be maintained longer at low temperatures (e.g., for months at -20 ^{o}C). The surface ionization, interparticle repulsion, and green luminescence of the ZnO QDs can, nevertheless, be greatly diminished by decreasing the polarity of the solvent. That is, upon the addition of a solvent mixture of isopropanol and hexane into the ZnO sol at a fixed ratio, the destabilized ZnO QDs form clusters and QD colloid immediately turned turbid at room temperature due to a weakened electrostatic repulsion.[82] The green luminescence of the turbid ZnO QD suspension is also significantly quenched owing to limited surface ionization and the reduced surface area (Fiugre 7.3, blue line).

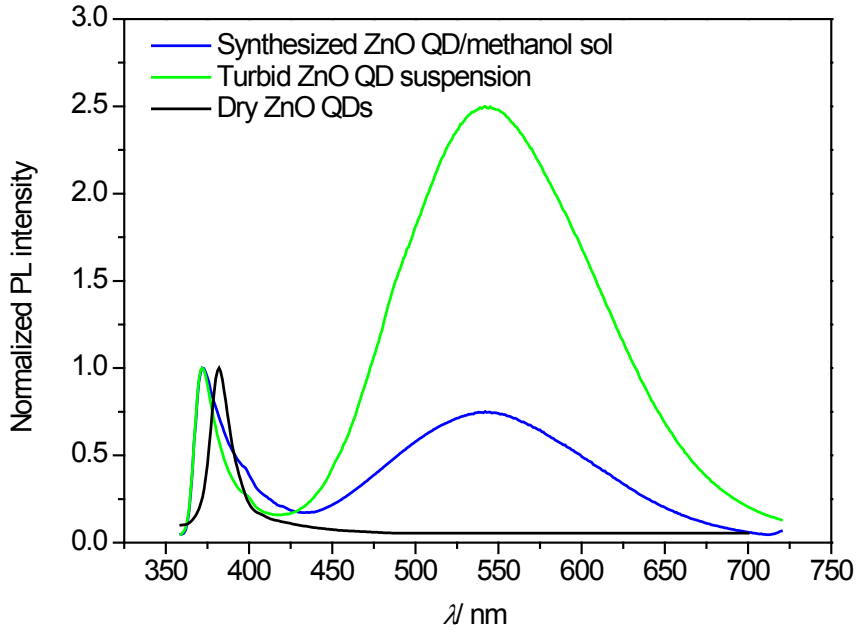

Figure 7.3. PL spectra of a synthesized ZnO sol, a turbid ZnO QD suspension upon addition of isopropanol and hexane and dry ZnO QDs.

In our experiments, this solvent-induced precipitation procedure was utilized to initialize the formation of colloidal crystals composed of surfactant-free ZnO QDs. by simply adjusting the $[K^+]$ in the synthesized ZnO sol, we have observed phase transitions of the surfactant-free ZnO QDs similar to that of microspheres. After resting overnight at 4 ^oC, the turbid ZnO suspension separated into two distinct phases. The upper phase consisted primarily of solvent while the lower one was a QD-rich condensed phase with morphologies varied at different ionic strength. Under high ionic strength, that is, when $[K^+]$ = 0.8 M, the lower phase became a gel-like fluid containing a high volume fraction

of ZnO QDs. The fluid remained transparent if undisturbed but turned turbid quickly under mechanical agitation. Therefore, this fluid is likely a long-range disordered structure (Figure 7.1B). At a lower ionic strength, such as $[K^+]$ = 0.4 M, the precipitated ZnO QDs formed a transparent solid layer, which has the same transparency as the gel structure, but can maintain stability even vigorously disturbed (Figure 7.1C). Hence, it could be easily separated from the supernatant without significant damage. This transparent layer will be demonstrated to be a colloidal crystal that exhibits an fcc-type structure later. Flocculation of ZnO QDs occurs at an even lower ionic strength ($[K^+]$ = 0.2 M), which is an amorphous structure with a white and loosely packed appearance (Figure 7.1D). Thus, by varying the ionic strength, it is possible to fine-tune the interparticle attractive potential on the kT scale in our system, which increases as the ionic strength decreases.

The above finding appears counterintuitive considering the ionic screening effect in a solution of high polarity where ion pairs are fully dissociated. The electrostatic double-layer repulsion between two identically charged particles falls progressively with salt addition, causing the interparticle attractive potential to increase as the electrolyte concentration rises in a solvent like water.[3] However, the surface ionization of a charged particle in a nonpolar solvent can be suppressed to an extent that a particle carries at most one or two charges.[83] Thus, in a nonpolar media, such as the mixture of hexane and alcohol used in our experiments, the ionic-screening effect is negligible. On the other hand, the effect of salt addition in a nonpolar solvent can be viewed as an increase in the polarity of the solution,[84] thereby enhancing the surface ionization and

the electrostatic interaction, and consequently causing a decrease in the total attractive potential. An ensuring fact of the theory is that when [K^+] is increased to 1.8 M, the polarity of the alcohol phase is so high that hexane and alcohol are no longer miscible. Right below the point of phase separation of the solvent, the ZnO QDs do not precipitate upon the addition of hexane and isopropanol because the electrostatic repulsion is now strong enough to maintain the ZnO QDs in a dispersed state ([K^+] = 1.6 M, Figure 7.1A).

7.4.2 Optical Spectroscopy—The Formation of QD Colloidal Crystal

The dimensions of the colloidal crystal prepared using this method can be easily controlled by choices of the container size and the concentration of the ZnO QDs. Figure 7.4 shows visual images of a white ZnO QD aggregate sample prepared by directly drying the ZnO–methanol solution for comparison purposes (Figure 7.4A), centimeter-sized transparent ZnO QD crystalline fragments (Figure 7.4B), a piece of transparent ZnO QD crystalline material with a thickness of 1 mm (Figure 7.4C), and a crystalline thin-film sample of ZnO QDs with a thickness of about 1 mm deposited on a piece of cover glass (2 cm x 2 cm) (Figure 7.4D).

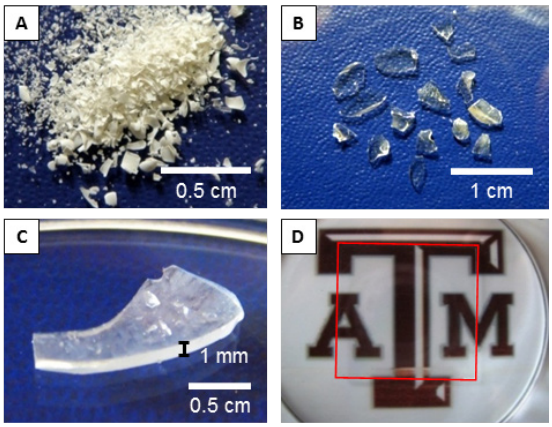

Figure 7.4. Photographical images of (A) white ZnO QD aggregates, (B) ZnO QD crystalline fragments, (C) 1 mm-thick ZnO QD crystalline solid and (D) a ZnO QD crystalline thin-film sample (outlined by the red square) deposited on a 2 cm x 2 cm cover glass.

The structure of the ZnO colloidal crystal in the thin film obtained upon annealing was studied. Once isolated from the colloidal solution, the sample was immediately covered with a second piece of cover glass to minimize solvent evaporation. The structural change in the colloidal crystal was monitored using UV-vis spectroscopy during the drying process. As shown in Figure 7.5A, ZnO QDs dispersed in methanol have an absorption onset of 355 nm, which corresponds to ZnO QDs of about 5.0 ± 0.3 nm in size.[85] The absorption onset of the deposited thin film right after removal from the solution was 365 nm, which had been significantly red-shifted, suggesting the formation of collective electronic states between interacting ZnO QDs.[86] After

annealing at room temperature for 30 min, 12 hours, 24 hours and 72 hours, the absorption onset was gradually shifted to 366, 370, and 371 nm, and to the absorption onset of bulk ZnO at 373 nm.[87] The absorption onset remained at this value even after prolonged annealing. This finding indicates that ZnO QDs within the colloidal crystal are spaced slightly farther apart from each other during the initial formation of the crystallite structures, most likely due to trapped residual solvent between the QDs. After slow evaporation of the entrapped solvent, the spacing between ZnO QDs reduces, and finally ZnO QDs make direct contact with each other to form a close-packed crystal structure after complete drying.[86, 88] Figure 7.5B shows the UV-vis transmission spectra of a ZnO QD dispersion in methanol, a ZnO crystalline QD thin film, and ZnO QD aggregates. The ZnO QD crystalline thin film with a thickness of about 1 mm exhibits nearly 100% transparency in the visible-light range. After drying, there is a slight drop in transparency, mainly due to crystal cracking caused by the process. In comparison to ZnO QD aggregates, the ZnO QD crystalline thin film shows negligible light scattering. It is transparent in the range of visible light and is capable of blocking UV light in the same manner as bulk ZnO.

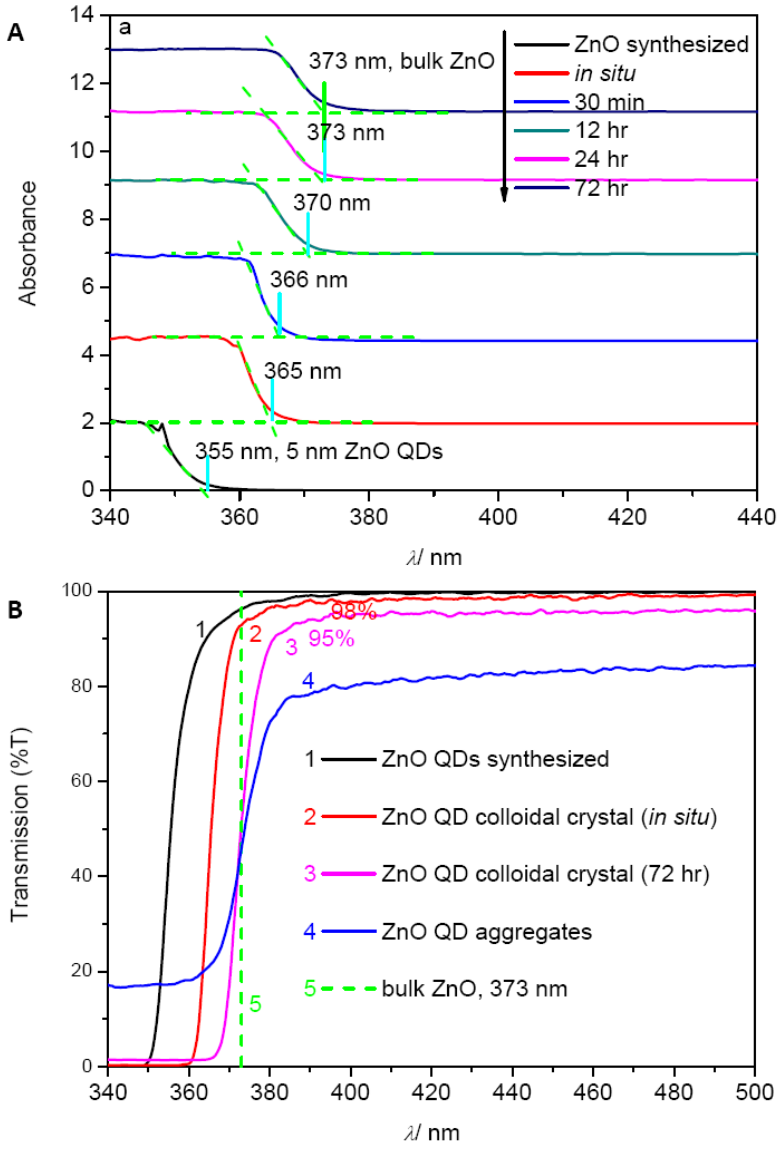

Figure 7.5. UV-Vis spectra. (A) Absorption spectra (normalized and offset vertically for clarity) of a synthesized ZnO QD sol, self-assembled crystalline structure in its wet state and after annealing for 0.5, 12, 24 and 72 hours. The dotted lines indicate the absorption onset. (B) Transmission spectra of a synthesized ZnO QD sol, a ZnO QD crystalline thin film (wet and after annealing) and of QD aggregates.

7.4.3 Structural Characterization

SAXS was utilized to investigate the internal structure of the above transparent ZnO QD solid. In Figure 7.6, SAXS 2D images of ZnO QD aggregates and a transparent solid are presented, and the SAXS intensity versus the scattering vector, $q = (4\pi/\lambda)\sin(\theta/2)$, is plotted, where λ is the wavelength of the incident Cu-Ka X-ray and θ is the scattering angle. The SAXS image of the transparent ZnO QD solid contains two distinct diffraction rings and the corresponding SAXS spectrum shows pronounced Bragg's diffraction peaks, whereas those for ZnO QD aggregates exhibit an amorphous characteristic. The diffraction peaks have a broadening feature similar to that for supracrystals of Au NPs reported in ref. [31], which should be due to various factors, such as defects, deformation, and the presence of an amorphous phase in the crystalline domains.[31] Subtracting the spectrum of the ZnO QD aggregates as the background, the spectrum of the transparent QD solid fits with two resolved peaks located at $q_1 = 0.139$ and $q_2 = 0.162$ Å^{-1}, with $q_2/q_1 = \sqrt{(4/3)}$. This diffraction pattern is characteristic of an fcc structure with a lattice constant **a** = 7.76 nm and an interparticle distance 2**r** =5.49 nm. The experimental and theoretical Bragg diffractions specified by the Miller indices are presented in the inset and agree to each other well. The observed fcc structure meets the requirement for optimizing interaction energies in a single-component system.[89] XRD and TEM both show that the average diameter of the synthesized ZnO QDs is around 5.3 nm (Figures 7.2 and 7.7). Therefore, the calculated interparticle distance corresponds to a close-packed structure of QDs in contact.

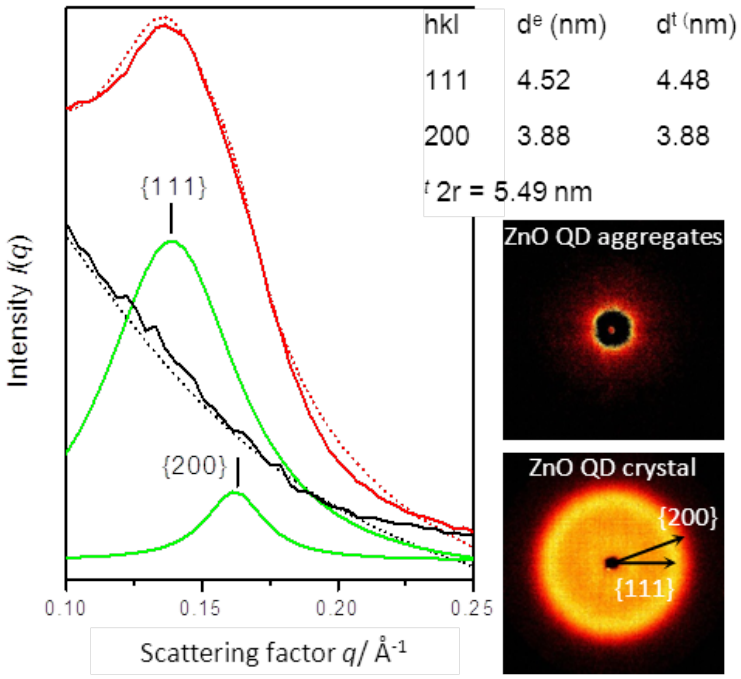

Figure 7.6. SAXS images and spectra of ZnO QD aggregates (black line) and ZnO QD colloidal crystals (red line). The dotted lines are the fits to experimental data. The green lines have the individual diffraction peaks resolved for the crystalline sample. The corresponding Bragg diffractions identified by Miller indices are presented in the inset.

7.4.4 Microscopy

SEM imaging was carried out to further investigate the crystalline characteristics of the ZnO QD assemblies. After being exposed to the electron beam during SEM imaging, sharp cracks formed in the crystalline material and propagated in a zigzag fashion perpendicular to the crack propagation direction (Figure 7.7A). The ZnO QD crystal also displayed multiple sharp rectangular corners (Figure 7.7B). This cracking

pattern is consistent with an fcc-type crystalline structure. The crystal surface was extremely smooth, making it difficult to observe individual ZnO QDs and their structure using SEM. On a rougher fracture surface, individual particles could be seen as closepacked (Figure 7.7C). In contrast, ZnO QD aggregates showed a rough surface and a porous morphology (Figure 7.7D), as would be expected for an amorphous structure.

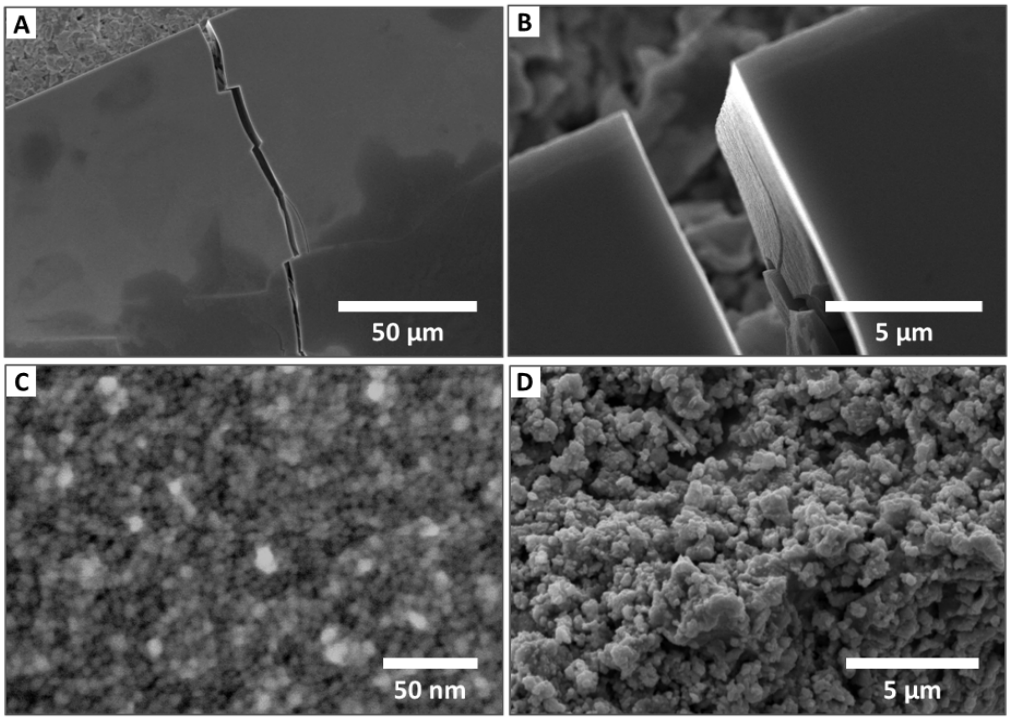

Figure 7.7. SEM micrographs of (A) a centimeter-sized ZnO QD colloidal crystal and the vertical and upright cracks formed under the SEM electron beam on the surface, (B) the rectangular corners at the crystal edge, (C) close-packed ZnO QDs of a size of about 5 nm on the crystal surface and (D) amorphous ZnO QD aggregates.

After grinding both the ZnO QD crystalline material and the amorphous QD aggregate into a fine powder and sonication in methanol, TEM shows that the ZnO QD crystal powder maintained a closepacked morphology (Figure 7.8A). Careful inspection of a crystal fragment revealed that ZnO QDs with a diameter of about 5.3 nm were stacked into multiple layers (Figure 7.8B). In contrast, the ZnO QD aggregates became randomly dispersed QDs and loosely formed clusters after grinding and sonication in methanol (Figure 7.8C).

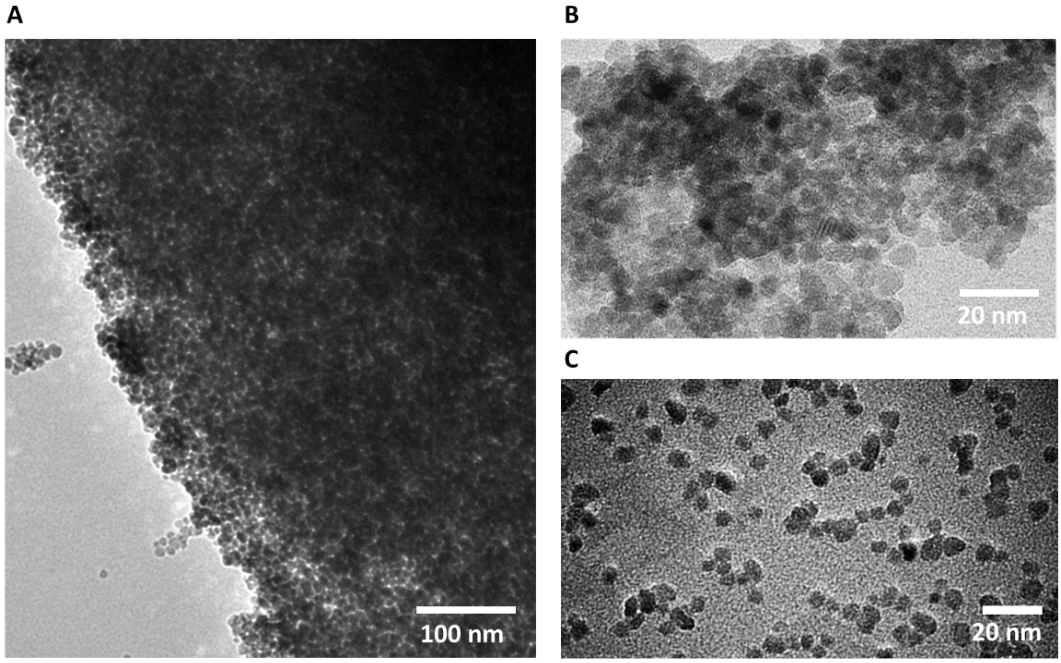

Figure 7.8. TEM micrographs of (A) the close-packed structure of ZnO QD colloidal crystal after being ground into powder and sonication in methanol, (B) close-packed ZnO QDs at the edge of the crystalline grains and (C) amorphous ZnO QD aggregates collapsed into randomly dispersed QDs after grinding and sonication in methanol.

7.5 Conclusions

It is found that colloidal ZnO QDs synthesized in methanol can form a variety of condensed phases by adding a mixture of hexane and isopropanol. Under different ionic strengths, the morphology of the condensed phase of ZnO QDs can be tuned to become flocculated agglomerates, a transparent gel-like fluid, or a transparent crystalline solid. The transparent colloidal crystalline phase is stable and can be isolated for structural characterization. A SAXS diffraction pattern of the crystalline phase suggests an fcc structure. UV-Vis, SEM and TEM were also performed to characterize this transparent ZnO QD solid. The ZnO QD crystalline material is transparent to visible light and absorbs UV light at 373 nm. The ZnO QD crystalline thin film may serve as a transparent UV-shielding material with many viable commercial device applications. The present study is also of particular significance for modeling the interaction and assembly of spherical colloidal particles at the nanoscale with tunable potentials.

CHAPTER VIII

CONCLUDING REMARKS AND FUTURE RECOMMENDATIONS

The research efforts in this dissertation include: (**i**) isolation of individually dispersed SWCNTs from the nanoplatelet dispersant, (**ii**) dispersion of purified NPs in solvents without using surfactants and (**iii**) investigation of the assembling behavior of a model NP.

Two effective methods for isolating the individual SWCNTs from the nanoplatelet dispersant have been developed and systematically studied. With the aid of appropriate surfactants, the ZrP nanoplatelets can be precipitated and removed from the system while the SWCNTs are stabilized. Special attention has been placed on the investigation of the electrostatic interaction of the SWCNTs and the nanoplatelets, the aggregation mechanism of the nanoplatelets, and the structural integrity and exfoliation state of SWCNTs before and after isolation.

The purified SWCNTs, along with other two types of NPs with different geometries (ZnO QDs and ZrP nanoplatelets), have been stabilized in an appropriate binary (or single-component) solvent without the use of surfactants. The NPs are stabilized through the minimization of vdW attraction, which is accomplished by matching the dielectric constants of the media and the NPs.

Purified ZnO QDs have been manipulated to shown a phase behavior similar to that of micro-spheres, with one crystalline phase that has an fcc structure and transparent

to visible light. The phase transition is tuned by adjusting the media ionic strength, thus varying the NP electrostatics and interparticle potential.

8.1 Isolation of Individual SWCNTs from the Nanoplatelet Dispersant

Individually dispersed SWCNTs have been isolated from the nanoplatelet dispersant through (1) an electrostatically controlled approach (an inonic approach) or (2) an acid mediated approach. The ionic approach requires the use of appropriate amount of cations to precipitate the ZrP and uses non-ionic surfactants to stabilize the SWCNTs. The approach has been optimized, resulting an extremely high yield (>90%) of individually dispersed SWCNTs. Two different working mechanisms have been determined for monovalent and divalent cations, respectively: the former works through the ionic screening effect and the latter induce the aggregation of ZrP by ion-exchanging.

The acid-mediated method enables the use of anionic surfactants to stabilize SWCNTs, while the ZrP is precipitated by a small amount of acid and allows for subsequent functionalization and transferring of the CNTs into various media. Compared with non-ionic surfactants, alkyl sulfate surfactant (SDS) can be used to reduce the required amount of extra acids. Generally, the acid-mediated approach yields about 80% individual SWNTs that are stabilized by the anionic or non-ionic surfactants. In comparison to the ionic approach, more SWCNTs are trapped in the precipitated ZrP, which is likely due to the relatively more compact structure of ZrP formed under the effect of acids.

8.2 Dispersion of Purified NPs

All three types of purified NPs (0-D ZnO QDs, 1-D SWCNTs and 2-D ZrP nanoplatelets), have been dispersed into various solvents possessing different dielectric constants. It is demonstrated that a dielectric-constant-matched solvent can provide long-term stability for the NPs through the minimization of the vdW attraction. NPs are unstable in solvents with larger or smaller ε values. Hamaker summation principle and DLP theory have been used to explain the phenomena. The dielectric properties of small NPs appear to be different from that of bulk materials, probably due to their increased reactivity, that is, the presence of surface defects renders the whole NPs more polar and reactive. Also, the differences seem to decrease as the NP particle size increases.

8.3 Controlled Assembly of Purified NPs

Colloidal ZnO QDs with a nearly uniform particle size of 5 nm have been synthesized and precipitated into a condensed phase in an organic solvent mixture without the use of surfactants. By adjusting the ionic strength of the solvent media, the interparticle potential of ZnO QD colloids can be tuned progressively to become repulsive or attractive to various degrees. This leads to the formation of distinct condenses phases of ZnO QDs with morphologies ranging from a white flocculation, to a gel-like fluid, and to a transparent solid. The transparent ZnO QD solid has 3-D crystalline characteristics. After solvent removal in atmosphere, the crystalline ZnO QD sheet exhibits a UV-shielding ability comparable to bulk ZnO while maintaining its

optical transparency and structural integrity. The phase transition is similar to that established for micro-spheres, and is observed with NPs for the first time.

8.4 Recommendations for Future Work

In order to further verify the applicability of the approaches developed and the phenomena observed in this dissertation, the following work is suggested.

8.4.1 Isolation of the SWCNTs from the Nanoplatelet Dispersant

i. The Electrostatically Controlled Method

In Chapter IV, we have shown that, while KCl almost causes instantaneous precipitation of ZrP, it reduces the yield of SWCNTs. It is possible that the big cation size (compared with Na^+) affects the stability of the non-ionic surfactants through the dehydration effect.[63] In this dissertation, most salts used to precipitate the ZrP are chloride. Potassium nitrate (KNO_3) and potassium bromide (KBr) have been reported to be able to stabilize non-ionic surfactants in comparison to KCl.[63] Therefore, the effect of anions in the ionic approach should be investigated, and could possibly leads to fast SWCNT-ZrP separation without a significant SWCNT loss.

ii. The Acid-Mediated approach

While SDS has been demonstrated effective in isolating the SWCNTs from ZrP, with a less requirement on acid addition compared with TX-100, it has been realized that SDS has a tendency to solubilize impurities more than to SWCNTs.[90] Another alkyl sulfate surfactant that can replace the use of SDS in this approach would be desirable.

8.4.2 Dispersion of Purified NPs

The hard sphere model predicts that the phase behavior of non-interacting sphere-like particles is solely dependent on the volume fraction of the NPs in the media.[12b, 75] However, the phenomenon has only been observed for micro-spheres. Current technique of manipulating NPs often involves the use of surfactants, which tend to complicate the assembling behavior of NPs. The purified ZnO QDs dispersed in methanol as prepared in Chapter VI, could be a model NP to investigating the intrinsic thermodynamics of NPs, and may exhibit a hard-sphere nature. This conjecture is made based on the following assumptions: (1) the vdW attraction can be minimized by matching the dielectric constant of the media and the QDs; (2) in nonpolar solvent, the surface ionization of QDs is suppressed significantly,[83] thereby minimizing the electrostatic repulsion; (3) the purified ZnO QDs carry no or limited conjugated surfactants (or ligand) on the surface; steric repulsion or hydrophobic attraction, which is usually caused by surfactants, is unlikely to occur; and (4) the effect of gravity may be temporarily compensated by the fast kinetics of NPs. However, in order to reach a volume fraction of certain transitions, for example, liquid-solid transition occurs at φ = 0.494,[12b, 75] the challenge is to prevent the further growth or aggregation of QDs during the removal of extra solvent.

8.4.3 Application of the Isolated SWCNTs

The SWCNTs isolated from the nanoplatelet dispersant remain individually dispersed, which provides the possibility of further purification of the SWCNTs by removing the catalyst residue. In the ionic approach, water-soluble polymeric surfactants

may be used to retrieve the SWCNTs and nanocomposites based on these water-soluble polymers and SWCNTs may be directly prepared from the SWCNT-enriched supernatants after SWCNT-ZrP separation to achieve a high concentration of well-dispersed SWCNTs. The functionalization of individual SWCNTs in SDS solution can also be utilized to prepare various types of polymer/SWCNT nanocomposites.

REFERENCES

[1] K. Kimura, *The Journal of Physical Chemistry* **1994**, *98*, 11997-12002.

[2] P. C. Hiemena, R. Rajagopalan, *Principles of Colloid and Surface Chemistry*, 3rd ed., Marcel Dekker, Inc., New York, **1997**.

[3] J. Israelachvili, *Intermolecular & Surface Forces*, 2nd ed., Academic Press, London, UK, **1991**.

[4] P. Bihari, M. Vippola, S. Schultes, M. Praetner, A. Khandoga, C. Reichel, C. Coester, T. Tuomi, M. Rehberg, F. Krombach, *Particle and Fibre Toxicology* **2008**, *5*, 14.

[5] a) M. Hernán, M. Francisco, L. Cefe, B. Álvaro, S. M. José, R. Joaquín, M. Amparo, F. Vicente, *Advanced Materials* **1998**, *10*, 480-483; b) Z. Wang, C. T. Chan, W. Zhang, N. Ming, P. Sheng, *Physical Review B* **2001**, *64*, 113108; c) J. E. Wijnhoven, W. L. Vos, *Science* **1998**, *281*, 802-804.

[6] a) K. C. Grabar, P. C. Smith, M. D. Musick, J. A. Davis, D. G. Walter, M. A. Jackson, A. P. Guthrie, M. J. Natan, *Journal of the American Chemical Society* **1996**, *118*, 1148-1153; b) D. L. Klein, R. Roth, A. K. L. Lim, A. P. Alivisatos, P. L. McEuen, *Nature* **1997**, *389*, 699-701.

[7] a) R. M. H. New, R. F. W. Pease, R. L. White*, Journal of Vacuum Science & Technology B: Microelectronics and Nanometer Structures* **1995**, *13*, 1089-1094; b) J. Shi, S. Gider, K. Babcock, D. D. Awschalom, *Science* **1996**, *271*, 937-941.

[8] a) Y. Volokitin, J. Sinzig, L. J. de Jongh, G. Schmid, M. N. Vargaftik, I. I. Moiseevi, *Nature* **1996**, *384*, 621-623; b) Z. L. Wang, J. M. Petroski, T. C.

Green, M. A. El-Sayed, *The Journal of Physical Chemistry B* **1998**, *102*, 6145-6151.

[9] D. Thompson, *Gold Bulletin* **2007**, *40*, 267-269.

[10] a) J. Turkevich, *Gold Bulletin* **1985**, *18*; b) J. Turkevich, *Gold Bulletin* **1985**, *18*.

[11] a) R. Garuthara, M. Tomkiewicz, R. Tenne, *Physical Review B* **1985**, *31*, 7844-7849; b) T. Okamoto, I. Yamaguchi, *The Journal of Physical Chemistry B* **2003**, *107*, 10321-10324; c) A. W. Snow, H. Wohltjen, *Chemistry of Materials* **1998**, *10*, 947-949.

[12] a) V. J. Anderson, H. N. W. Lekkerkerker, *Nature* **2002**, *416*, 811-815; b) P. N. Pusey, W. van Megen, *Nature* **1986**, *320*, 340-342; c) W. B. Russel, *Nature* **2003**, *421*, 490-491.

[13] S. Iijima, *Nature* **1991**, *354*, 56-58.

[14] a) J. P. Salvetat, J. M. Bonard, N. H. Thomson, A. J. Kulik, L. Forro, W. Benoit, L. Zuppiroli, *Applied Physics A: Materials Science & Processing* **1999**, *69*, 255; b) M. M. J. Treacy, T. W. Ebbesen, J. M. Gibson, *Nature* **1996**, *381*, 678-680.

[15] a) J. Hone, M. Whitney, C. Piskoti, A. Zettl, *Physical Review B* **1999**, *59*, R2514; b) M. A. Osman, D. Srivastava, *Nanotechnology* **2001**, *12*, 21-24.

[16] a) H. Dai, E. W. Wong, C. M. Lieber, *Science* **1996**, *272*, 523-526; b) T. W. Ebbesen, H. J. Lezec, H. Hiura, J. W. Bennett, H. F. Ghaemi, T. Thio, *Nature* **1996**, *382*, 54-56.

[17] M. J. O'Connell, S. M. Bachilo, C. B. Huffman, V. C. Moore, M. S. Strano, E. H. Haroz, K. L. Rialon, P. J. Boul, W. H. Noon, C. Kittrell, J. Ma, R. H. Hauge, R. B. Weisman, R. E. Smalley, *Science* **2002**, *297*, 593-596.

[18] E. Pop, D. Mann, Q. Wang, K. Goodson, H. Dai, *Nano Letters* **2005**, *6*, 96-100.

[19] a) M. J. Biercuk, M. C. Llaguno, M. Radosavljevic, J. K. Hyun, A. T. Johnson, J. E. Fischer, *Applied Physics Letters* **2002**, *80*, 2767-2769; b) M. B. Bryning, M. F. Islam, J. M. Kikkawa, A. G. Yodh, *Advanced Materials* **2005**, *17*, 1186-1191; c) L. Sun, G. L. Warren, J. Y. O'Reilly, W. N. Everett, S. M. Lee, D. Davis, D. Lagoudas, H. J. Sue, *Carbon* **2008**, *46*, 320-328.

[20] S. Wang, S. Sato, K. Kimura, *Chemistry of Materials* **2003**, *15*, 2445-2448.

[21] I. Ojea-Jiménez, F. M. Romero, N. G. Bastús, V. Puntes, *The Journal of Physical Chemistry C* **2010**, *114*, 1800-1804.

[22] a) W. Cheng, M. J. Campolongo, J. J. Cha, S. J. Tan, C. C. Umbach, D. A. Muller, D. Luo, *Nat Mater* **2009**, *8*, 519-525; b) L. Liu, K. Xu, H. Wang, T. Jeremy, W. Fan, S. S. Venkatraman, L. Li, Y. Y. Yang, *Nat Nano* **2009**, *4*, 457-463.

[23] A. Gudkova, K. Kienskaya, V. Nazarov, V. Kim, S. Mukhtarova, *Russian Journal of Applied Chemistry* **2005**, *78*, 1757-1760.

[24] C. B. Murray, D. J. Norris, M. G. Bawendi, *Journal of the American Chemical Society* **1993**, *115*, 8706-8715.

[25] a) P. de la Presa, M. Multigner, J. de la Venta, M. A. Garcia, M. L. Ruiz-Gonzalez, *Journal of Applied Physics* **2006**, *100*, 123915-123916; b) I. Lokteva,

N. Radychev, F. Witt, H. Borchert, J. r. Parisi, J. Kolny-Olesiak, *The Journal of Physical Chemistry C* **2010**, *114*, 12784-12791.

[26] Y. Wang, J. F. Wong, X. Teng, X. Z. Lin, H. Yang, *Nano Letters* **2003**, *3*, 1555-1559.

[27] a) A. Reindl, W. Peukert, *Journal of Colloid and Interface Science* **2008**, *325*, 173-178; b) S. K. Ghosh, S. Deguchi, S.-a. Mukai, K. Tsujii, *The Journal of Physical Chemistry B* **2007**, *111*, 8169-8174.

[28] A. Gupta, A. Khalil, M. Winterer, H. Wiggers, in *Nanoelectronics Conference (INEC), 2010 3rd International*, **2010**, pp. 1018-1019.

[29] D. Sun, M. Wong, L. Sun, Y. Li, N. Miyatake, H. J. Sue, *Journal of Sol-Gel Science and Technology* **2007**, *43*, 237-243.

[30] a) M. K. Corbierre, J. Beerens, J. Beauvais, R. B. Lennox, *Chemistry of Materials* **2006**, *18*, 2628-2631; b) T. Teranishi, A. Sugawara, T. Shimizu, M. Miyake, *J.Am.Chem.Soc.* **2002**, *124*, 4210-4211; c) M. N. Martin, J. I. Basham, P. Chando, S. K. Eah, *Langmuir* **2010**, *26*, 7410-7417.

[31] K. J. M. Bishop, B. A. Grzybowski, *Proceedings of the National Academy of Sciences* **2007**, *104*, 10305-10309.

[32] a) D. Nykypanchuk, M. M. Maye, D. van der Lelie, O. Gang, *Nature* **2008**, *451*, 549-552; b) S. Y. Park, A. K. R. Lytton-Jean, B. Lee, S. Weigand, G. C. Schatz, C. A. Mirkin, *Nature* **2008**, *451*, 553-556.

[33] C. A. Mirkin, *MRS Bulletin* **2010**, *35*, 532-539.

[34] a) C. B. Murray, C. R. Kagan, M. G. Bawendi, *Science* **1995**, *270*, 1335-1338; b) C. B. Murray, C. R. Kagan, M. G. Bawendi, *Annual Review of Materials Science* **2000**, *30*, 545; c) D. V. Talapin, E. V. Shevchenko, A. Kornowski, N. Gaponik, M. Haase, A. L. Rogach, H. Weller, *Advanced Materials* **2001**, *13*, 1868-1871; d) J. J. Urban, D. V. Talapin, E. V. Shevchenko, C. B. Murray, *J.Am.Chem.Soc.* **2006**, *128*, 3248-3255.

[35] a) J. Kong, H. T. Soh, A. M. Cassell, C. F. Quate, H. Dai, *Nature* **1998**, *395*, 878-881; b) X. Liu, J. Ly, S. Han, D. Zhang, A. Requicha, M. E. Thompson, C. Zhou, *Advanced Materials* **2005**, *17*, 2727-2732.

[36] a) T. H. Kim, C. Doe, S. R. Kline, S. M. Choi, *Macromolecules* **2008**, *41*, 3261-3266; b) S. Qin, D. Qin, W. T. Ford, J. E. Herrera, D. E. Resasco, *Macromolecules* **2004**, *37*, 9963-9967; c) G. Viswanathan, N. Chakrapani, H. Yang, B. Wei, H. Chung, K. Cho, C. Y. Ryu, P. M. Ajayan, *Journal of the American Chemical Society* **2003**, *125*, 9258-9259.

[37] a) T. Dimitrios, T. Nikos, G. Vasilios, P. Maurizio, *Chemistry - A European Journal* **2003**, *9*, 4000-4008; b) L. A. Girifalco, M. Hodak, R. S. Lee, *Physical Review B* **2000**, *62*, 13104.

[38] a) J. M. Ashcroft, K. B. Hartman, Y. Mackeyev, C. Hofmann, S. Pheasant, L. B. Alemany, L. J. Wilson, *Nanotechnology* **2006**, *17*, 5033; b) F. Liang, J. M. Beach, P. K. Rai, W. Guo, R. H. Hauge, M. Pasquali, R. E. Smalley, W. E. Billups, *Chemistry of Materials* **2006**, *18*, 1520-1524; c) B. K. Price, J. M. Tour, *Journal of the American Chemical Society* **2006**, *128*, 12899-12904.

[39] V. C. Moore, M. S. Strano, E. H. Haroz, R. H. Hauge, R. E. Smalley, J. Schmidt, Y. Talmon, *Nano Letters* **2003**, *3*, 1379-1382.

[40] a) J. Chen, H. Liu, W. A. Weimer, M. D. Halls, D. H. Waldeck, G. C. Walker, *Journal of the American Chemical Society* **2002**, *124*, 9034-9035; b) A. Star, J. F. Stoddart, D. Steuerman, M. Diehl, A. Boukai, E. W. Wong, X. Yang, S.-W. Chung, H. Choi, J. R. Heath, *Angewandte Chemie International Edition* **2001**, *40*, 1721-1725; c) M. J. O'Connell, P. Boul, L. M. Ericson, C. Huffman, Y. Wang, E. Haroz, C. Kuper, J. Tour, K. D. Ausman, R. E. Smalley, *Chemical Physics Letters* **2001**, *342*, 265-271.

[41] a) M. Zheng, A. Jagota, E. D. Semke, B. A. Diner, R. S. McLean, S. R. Lustig, R. E. Richardson, N. G. Tassi, *Nat Mater* **2003**, *2*, 338-342; b) M. E. Hughes, E. Brandin, J. A. Golovchenko, *Nano Letters* **2007**, *7*, 1191-1194.

[42] a) D. Changwoo, C. Sung-Min, R. K. Steven, J. Hyung-Sik, K. Tae-Hwan, *Advanced Functional Materials* **2008**, *18*, 2685-2691; b) D. Sun, W. N. Everett, C. C. Chu, H. J. Sue, *Small* **2009**, *5*, 2692-2697.

[43] A. Garg, S. B. Sinnott, *Chemical Physics Letters* **1998**, *295*, 273-278.

[44] B. Gebhardt, Z. Syrgiannis, C. Backes, R. Graupner, F. Hauke, A. Hirsch, *Journal of the American Chemical Society* **2011**, *133*, 7985-7995.

[45] a) T. S. Balaban, M. C. Balaban, S. Malik, F. Hennrich, R. Fischer, H. Rosner, M. M. Kappes, *Advanced Materials* **2006**, *18*, 2763-2767; b) N. Tagmatarchis, V. Georgakilas, M. Prato, H. Shinohara, *Chemical Communications* **2002**, 2010-

2011; c) R. Tian, X. Wang, Y. Xu, S. Li, L. Wan, M. Li, J. Cheng, *Journal of Nanoparticle Research* **2009**, *11*, 1201-1208.

[46] a) A. Clearfield, *Annual Review of Materials Science* **1984**, *14*, 205-229; b) L. Sun, W. J. Boo, H. J. Sue, A. Clearfield, *New Journal of Chemistry* **2007**, *31*, 39-43.

[47] H. N. Kim, S. W. Keller, T. E. Mallouk, J. Schmitt, G. Decher, *Chemistry of Materials* **1997**, *9*, 1414-1421.

[48] X. Zhang, T. V. Sreekumar, T. Liu, S. Kumar, *The Journal of Physical Chemistry B* **2004**, *108*, 16435-16440.

[49] J. E. Riggs, Z. Guo, D. L. Carroll, Y. P. Sun, *Journal of the American Chemical Society* **2000**, *122*, 5879-5880.

[50] D. Sun, C. C. Chu, H. J. Sue, *Chemistry of Materials* **2010**, *22*, 3773-3778.

[51] J. Liu, A. G. Rinzler, H. Dai, J. H. Hafner, R. K. Bradley, P. J. Boul, A. Lu, T. Iverson, K. Shelimov, C. B. Huffman, F. Rodriguez-Macias, Y. S. Shon, T. R. Lee, D. T. Colbert, R. E. Smalley, *Science* **1998**, *280*, 1253-1256.

[52] L. V. Basbanes, ed., *Advanced Materials Research Trends*, Nova Publishers, New York, **2007**.

[53] Y. Lin, D. E. Hill, J. Bentley, L. F. Allard, Y. P. Sun, *The Journal of Physical Chemistry B* **2003**, *107*, 10453-10457.

[54] a) S. D. M. Brown, A. Jorio, M. S. Dresselhaus, G. Dresselhaus, *Physical Review B* **2001**, *64*, 073403; b) U. D. Venkateswaran, A. M. Rao, E. Richter, M. Menon,

A. Rinzler, R. E. Smalley, P. C. Eklund, *Physical Review B* **1999**, *59*, 10928-10934.

[55] a) R. Saito, G. Dresselhaus, M. S. Dresselhaus, *Physical Review B* **2000**, *61*, 2981; b) R. B. Weisman, S. M. Bachilo, D. Tsyboulski, *Applied Physics A: Materials Science & Processing* **2004**, *78*, 1111-1116.

[56] a) C. A. Dyke, J. M. Tour, *The Journal of Physical Chemistry A* **2004**, *108*, 11151-11159; b) J. L. Stevens, A. Y. Huang, H. Peng, I. W. Chiang, V. N. Khabashesku, J. L. Margrave, *Nano Letters* **2003**, *3*, 331-336.

[57] A. J. Blanch, C. E. Lenehan, J. S. Quinton, *The Journal of Physical Chemistry B* **2010**, *114*, 9805-9811.

[58] S. Niyogi, S. Boukhalfa, S. B. Chikkannanavar, T. J. McDonald, M. J. Heben, S. K. Doorn, *Journal of the American Chemical Society* **2007**, *129*, 1898-1899.

[59] a) P. W. Barone, S. Baik, D. A. Heller, M. S. Strano, *Nat Mater* **2005**, *4*, 86-92; bN. Izard, D. Riehl, E. Anglaret, *Physical Review B* **2005**, *71*, 195417; cT. J. McDonald, C. Engtrakul, M. Jones, G. Rumbles, M. J. Heben, *The Journal of Physical Chemistry B* **2006**, *110*, 25339-25346.

[60] a) M. J. Bronikowski, P. A. Willis, D. T. Colbert, K. A. Smith, R. E. Smalley, *Journal of Vacuum Science & Technology A: Vacuum, Surfaces, and Films*, **2001**, *19*, 1800-1805; b) W. Zhou, Y. H. Ooi, R. Russo, P. Papanek, D. E. Luzzi, J. E. Fischer, M. J. Bronikowski, P. A. Willis, R. E. Smalley, *Chemical Physics Letters* **2001**, *350*, 6-14.

[61] a) Z. Feldoto, T. Pettersson, A. Dedinaite, *Langmuir* **2008**, *24*, 3348-3357; b) R. M. Mason, R. W. Mayes, *Biochem.J.* **1973**, *131*, 535-540.

[62] a) A. Clearfield, H. Hagiwara, *Journal of Inorganic and Nuclear Chemistry* **1978**, *40*, 907-914; b) L. Kullberg, A. Clearfield, *The Journal of Physical Chemistry* **1981**, *85*, 1585-1589.

[63] a) H. Schott, A. E. Royce, *Journal of Pharmaceutical Sciences* **1984**, *73*, 793-799; b) H. Schott, A. E. Royce, *Colloids and Surfaces* **1986**, *19*, 399-418.

[64] K. L. White, M. Shuai, X. Zhang, H.-J. Sue, R. Nishimura, *Carbon* **2011**, *49*, 5124-5131.

[65] *pKa Data Compiled by R. William*; http://research.chem.psu.edu/brpgroup/pKa_compilation.pdf (accessed 01/17/12).

[66] a) J. L. Kurz, *The Journal of Physical Chemistry* **1962**, *66*, 2239-2246; b) V. A. Motsavage, H. B. Kostenbauder, *Journal of Colloid Science* **1963**, *18*, 603-615.

[67] B. Vigolo, A. Pénicaud, C. Coulon, C. Sauder, R. Pailler, C. Journet, P. Bernier, P. Poulin, *Science* **2000**, *290*, 1331-1334.

[68] a) W. J. E. Beek, M. M. Wienk, R. A. J. Janssen, *Advanced Materials* **2004**, *16*, 1009-1013; b) W. J. E. Beek, M. M. Wienk, R. A. J. Janssen, *Journal of Materials Chemistry* **2005**, *15*, 2985-2988.

[69] M. Wong, R. Tsuji, S. Nutt, H. J. Sue, *Soft Matter* **2010**, *6*, 4482-4490.

[70] V. P. Pawar, S. C. Mehrotra, *Journal of Solution Chemistry* **2002**, *31*, 577-588.

[71] W. Tjhen, T. Tamagawa, C. P. Ye, C. C. Hsueh, P. Schiller, D. L. Polla, in *Micro Electro Mechanical Systems, 1991, MEMS '91, Proceedings. An Investigation of*

Micro Structures, Sensors, Actuators, Machines and Robots. IEEE, Nara, Japan, **1991**, pp. 114-119.

[72] U. Kreibig, C. v. Fragstein, *Zeitschrift für Physik A Hadrons and Nuclei* **1969**, *224*, 307-323.

[73] R. L. David, ed., in *Bond Dissociation Energies in Diatomic Molecules*, *89th*, CRC Press, Florida, **2009**.

[74] E. W. Seelig, B. Tang, A. Yamilov, H. Cao, R. P. H. Chang, *Materials Chemistry and Physics* **2003**, *80*, 257-263.

[75] Z. Cheng, P. M. Chaikin, W. B. Russel, W. V. Meyer, J. Zhu, R. B. Rogers, R. H. Ottewill, *Materials & Design* **2001**, *22*, 529-534.

[76] W. B. Russel, D.A.Saville, W.R.Schowalter, *Colloidal Dispersion*, Cambridge Univeristy Press, Cambridge, UK, **1989**.

[77] B. A. Korgel, S. Fullam, S. Connolly, D. Fitzmaurice, *The Journal of Physical Chemistry B* **1998**, *102*, 8379-8388.

[78] R. D. Yang, S. Tripathy, Y. Li, H. J. Sue, *Chemical Physics Letters* **2005**, *411*, 150-154.

[79] D. W. Bahnemann, C. Kormann, M. R. Hoffmann, *The Journal of Physical Chemistry* **1987**, *91*, 3789-3798.

[80] a) A. van Dijken, E. A. Meulenkamp, D. Vanmaekelbergh, A. Meijerink, *Journal of Luminescence* **2000**, *90*, 123-128; b) K. Vanheusden, C. H. Seager, W. L. Warren, D. R. Tallant, J. A. Voigt, *Applied Physics Letters* **1996**, *68*, 403-405.

[81] M. Anpo, Y. Kubokawa, *The Journal of Physical Chemistry* **1984**, *88*, 5556-5560.

[82] N. Mishchuk, *Journal of Colloid and Interface Science* **2008**, *320*, 599-607.

[83] E. V. Shevchenko, D. V. Talapin, N. A. Kotov, S. O'Brien, C. B. Murray, *Nature* **2006**, *439*, 55-59.

[84] G. L. Huppert, B. C. Wu, S. H. Townsend, M. T. Klein, S. C. Paspek, *Industrial & Engineering Chemistry Research* **1989**, *28*, 161-165.

[85] a) L. Brus, *The Journal of Physical Chemistry* **1986**, *90*, 2555-2560; b) D. Sun, H. J. Sue, N. Miyatake, *The Journal of Physical Chemistry C* **2008**, *112*, 16002-16010.

[86] M. V. Artemyev, A. I. Bibik, L. I. Gurinovich, S. V. Gaponenko, U. Woggon, *Phys.Rev.B* **1999**, *60*, 1504.

[87] P. D. Cozzoli, M. L. Curri, A. Agostiano, G. Leo, M. Lomascolo, *The Journal of Physical Chemistry B* **2003**, *107*, 4756-4762.

[88] M. V. Artemyev, U. Woggon, H. Jaschinski, L. I. Gurinovich, S. V. Gaponenko, *The Journal of Physical Chemistry B* **2000**, *104*, 11617-11621.

[89] S. C. Mau, D. A. Huse, *Physical Review E* **1999**, *59*, 4396.

[90] W. Wenseleers, I. I. Vlasov, E. Goovaerts, E. D. Obraztsova, A. S. Lobach, A. Bouwen, *Advanced Functional Materials* **2004**, *14*, 1105-1112.

APPENDIX A

QUANTIFICATION OF CONCENTRATION OF WELL-DISPERSED SWCNTS IN SOLUTION

According to Beer–Lambert law, at a fixed wavelength (λ) of excitation light:

$$I = \epsilon l c$$

where I = absorption intensity, ϵ = scaling constant, l = light path length, and c = solute concentration.

The equation describes the linear dependence of absorption intensity on solute concentration. For SWCNTs obtained using the ionic approach as described in Chapter IV, assuming that SWCNT remains well dispersed before and after ZrP removal and at l = 10 mm, we have

$$I_1 = \epsilon_1 \text{ [SWCNT], at } \lambda_1$$

$$I_2 = \epsilon_2 \text{ [SWCNT], at } \lambda_2$$

$$I_1 - I_2 = (\epsilon_1 - \epsilon_2) \text{ [SWCNT]} = \epsilon \text{ [SWNT]}, \epsilon = \epsilon_1 - \epsilon_2$$

Here the difference between the absorption intensity at two different wavelengths is used to compensate the zero line shifting of the spectrometer. Absorption spectra of standard solutions of SWCNT/ZrP/TX-100 mixture with [SWCNT] = 20, 40, 60, 80 and 100 ppm are shown in Figure A1A. The linear fit of absorption intensity at λ_1 = 850 nm, denoted as I_1, absorption intensity at λ_2 = 1000 nm, denoted as I_2, and their intensity difference, denoted as $I_1 - I_2$, to [SWCNT] is shown in Figure A1B. The above wavelengths were chosen because the ZrP dispersant, TX-100 and ion exhibit zero

absorption and their existence does not affect the absorption intensity of SWCNT at those wavelengths. The linear fit of I_1, I_2 and $I_1 - I_2$ as a function of [SWCNT] yield R^2 = 0.99998, 0.99997, and 0.99999, respectively. Thus, this method is reliable for measuring [SWCNT].

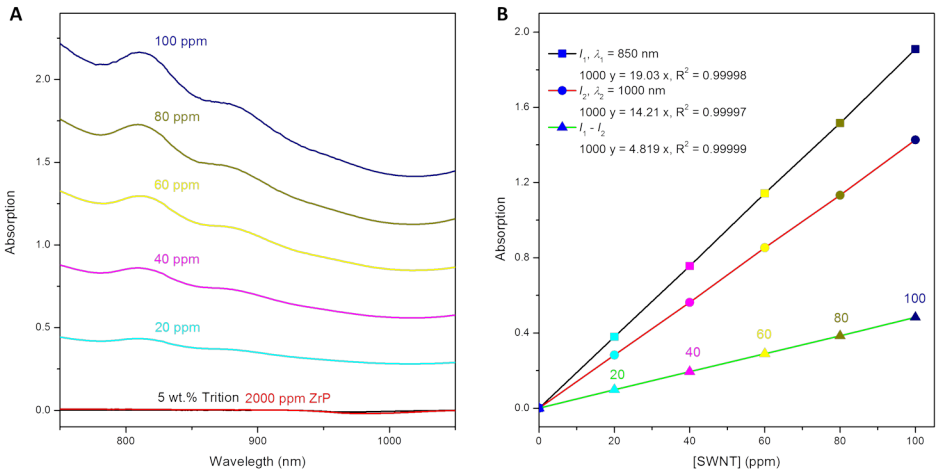

Figure A1. (A) UV-vis spectra of aqueous solutions of TX-100, ZrP exfoliated by TBA^+OH^-, and SWCNT/ZrP/TX-100 at various concentrations. (B) Linear fit of absorption intensity at different wavelengths versus [SWCNT].

After centrifugation, the SWCNT-enriched supernatant does not possess the same volume before salt addition because the precipitated ZrP also contains trapped water. Therefore, pure water was added to the supernatant to reach a known volume. By comparing the [SWCNT] (after SWCNT-ZrP separation) multiplied by the volume of the diluted supernatant against [SWCNT] (before separation) multiplied by the volume

of the SWCNT/ZrP/TX-100 dispersion, the yield of SWCNT in the supernatant can thus be quantified.

For SWCNTs obtained using the acid-mediated approach with SDS as the stabilizer, absorption intensity at λ = 742 nm is used to quantify the [SWCNT] instead of using the difference between the absorption intensity at two different wavelengths. The is because that the existence of SDS tends to exaggerate the intensity difference, especially in the range between 850 nm and 1000 nm.

APPENDIX B

A 2-IN-1 STEP OF FUNCTIONALIZATION AND STABILIZATION OF CNTS INTO ORGANIC MEDIA

The functionalization mechanisms and processes are depicted in Figure B1. A concentrated solution of sulfanilamide in acetone (10%), or other functionalizing agents was added into the SWCNT/SDS solutions based on a 1:1 stoichiometry of the amine groups on sulfanilamide and carboxylic groups on SWCNT (Figure B1A). The carbon and oxygen contents in CNT were roughly determined by EDS and XPS. The mixture was kept at 70 ^{o}C overnight and SWCNT form flocculation, indicating the surface functionalization rendering them insoluble in water phase (Figure B1B). SWCNT were then retrieved by filtration or centrifugation and extra SDS and unreacted sulfanilamide were washed away with alcohol. Acetone was used to re-disperse SWCNT with sonication (Figure B1C). SWCNT dispersion is found to be stable for at least 10 months. The CNT dispersion with a concentration > 600 ppm remains stable.

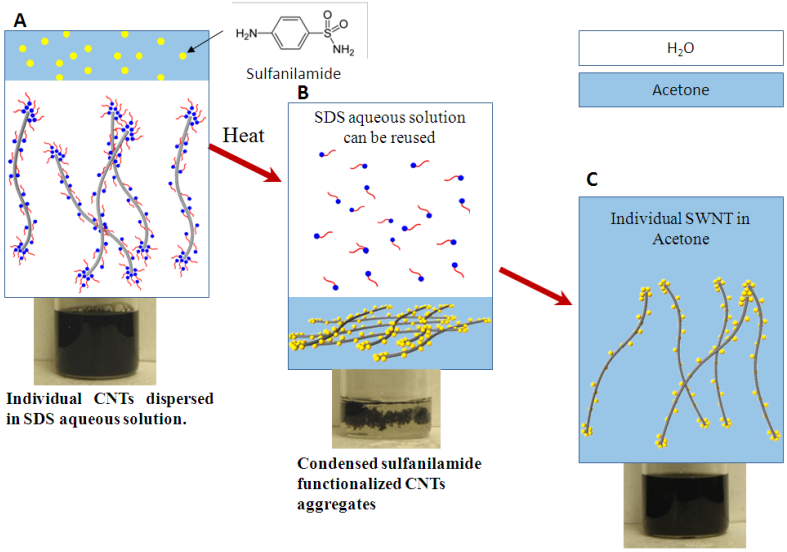

Figure B1. Conceptual and realistic illustration of functionalization and transfer of individual CNTs from aqueous solutions to organic systems. Sulfanilamide as a functionalization agent and acetone as a dispersing medium are shown as an example. (A) Concentrated acetone solution of sulfanilamide are added into SDS aqueous solution to functionalize individual CNTs. (B) CNTs functionalized with sulfanilamide become insoluble in water and are condensed into acetone phase to form flocculation. (C) CNTs aggregates are re-dispersed into acetone under sonication.

When MWCNTs were functionalized by octalymine using the above approach, conductive polypropylene nanocomposites based on MWCNT have been prepared with an electrical percolation threshold of CNT concentration among the lowest reported.

VITA

Xi Zhang received her bachelor's degree in materials physics and chemistry from Wuhan University in China in 2006. After one year of study on Bio-MEMS in Nanyang Technological University in Singapore, she entered the Materials Science and Engineering program at Texas A&M University. Her research interests include synthesis, dispersion and functionalization of nanoparticles, especially the dispersion and functionalization of carbon nanotubes. She became an industrial researcher in January 2012 and received her Ph.D. degree in May 2012. She writes essays and enjoys reading in her spare time.

Ms. Zhang may be reached at Polymer Technology Center, Texas A&M University, Texas 77843-3123. Her email is lifefantasy@gmail.com.